UNIVERSIDAD NACIONAL AUTÓNOMA DE MÉXICO

PROGRAMA DE MAESTRÍA Y DOCTORADO EN INGENIERÍA

INGENIERÍA MECÁNICA - DISEÑO MECÁNICO

ESTUDIO DE LA RELACIÓN DE PROPIEDADES MECÁNICAS Y MANUFACTURABILIDAD EN ESTRUCTURAS CONSTRUIDAS POR MANUFACTURA ADTIVA

TESIS

QUE PARA OPTAR POR EL GRADO DE:

DOCTOR EN INGENIERÍA

PRESENTA:

M.I. CASTRO ESPINOSA HOMERO ALBERTO

TUTOR

DR. LEOPOLDO RUIZ HUERTA

INSTITUTO DE CIENCIAS APLICADAS Y TECNOLOGÍA, UNAM

COMITÉ TUTOR

DR. VICENTE BORJA

FACULTAD DE INGENIERÍA, UNAM

DR. FERNANDO VELÁZQUEZ

FACULTAD DE INGENIERÍA,UNAM

DR. HÉCTOR RAFAEL SILLER CARRILLO

UNIVERSITY OF NORTH TEXAS

DR. CIRO RODRÍGUEZ

TECNOLÓGICO DE MONTERREY, NUEVO LEÓN

CIUDAD UNIVERSITARIA, CDMX, SEPTIEMBRE 2023

JURADO ASIGNADO:

Presidente: Dr. Borja Ramírez Vicente

Secretario: Dr. Velázquez Villegas Fernando

1er. Vocal: Dr. Ruiz Huerta Leopoldo

2do. Vocal: Dr. Héctor Rafael Siller Carrillo

3er. Vocal: Dr. Rodríguez González Ciro Ángel

Lugar donde se realizó la tesis: Laboratorio Nacional de Manufactura Aditiva y Digital (MADiT) del Instituto de Ciencias Aplicadas y Tecnología (ICAT)ubicado en Ciudad Universitaria, Universidad Nacional Autónoma de México (UNAM).

TUTOR DE TESIS:

Dr. Leopoldo Ruiz Huerta

This doctoral research was developed in the facilities of the National Laboratory of Additive and Digital Manufacturing (MADiT), at its headquarters in the Institute of Applied Sciences and Technology (ICAT) located in Universidad Nacional Autónoma de México (UNAM).

This work has been supported by the Consejo Nacional de Humanidades, Ciencias y Tecnologías (CONACHyT) through a scholarship number 722170 with CVU 665646, awarded for PhD studies, and grants LN315910, LN314934, LN299129 and DGAPA PAPIIT project IT102423.

Abstract

Additive manufacturing allows the construction of complex shapes such as heat exchangers, porous and optimized structures etc. Particularly, Laser Powder Bed Fusion for Metallic alloys (LPBF-M) enables the construction of metallic components. Among the many structures that are possible, metallic lightweight structures have found a place in industries such as medical, aerospace, automotive and energy fields. Nevertheless, certain structures contain elements such as thin and inclined walls, and struts that stretch the capabilities of the process. This, combined with the variability that exists in LPBF, are cause of a wide range of process parameters and material conditions for each LPBF-M machine brand, and makes uncertain whether a structure is manufacturable or not, since a part that is manufacturable in one machine, may not necessarily be in another. In this thesis, manufacturability is studied through a material-process approach in which the minimum unit of the process, e.g. the melting pool, generated by the material and process parameters, is compatible with the desired geometry to build. According to this approach, it is enabled the possibility of knowing the manufacturability of a lightweight structures according to the available material conditions and the process parameters employed.

Contents

List of Figures

List of Tables

Introduction

Additive Manufacturing (AM) enables component constructions through layer-by-layer deposition, unlike conventional substractive manufacturing. Due to its nature of constructing additively, AM has certain advantages such as: cost improvement for small volumes, fabrication environment impact reduction and capacity increase to build complex structures without extra tools, this is why AM is considered a disruptive technology [1].

Among the AM processes, is the Laser Powder Bed Fusion for Metallic alloys (LPBF-M). Within all the possibilities that this process can build, complex metallic components like reticulated structures, shock absorbers, heat exchangers, acoustic absorbers and lightweight structures have been successfully constructed [2].

Literature research has identified, that in the LPBF-M process, there is a considerable material conditions and process parameter that depend specifically on each machine. This not only causes variability in mechanical properties, but also uncertainty on whether a structure, like a lightweight structure, is manufacturable or not, because being succesfully manufacturable in one specific equipment, does not mean to be necessarily so on another. This is known in literature as Manufacturability and is defined as the design and characteristics which indicate how difficult or easy the design is from a manufacturing perspective. Variability in either mechanical properties or manufacturability, has caused the process to not meet standardization requirements that conventional manufacturing processes currently have, which is holding back the adoption of this technology at the industrial level.

Variability occurs because there are different combinations, a result of using different

material conditions and process parameters that depend on the machine employed, leading in the final component to different cooling rates, microstructures, residual stress and defects, among others.

Based on this condition, in this thesis document, it is studied the material-process interaction that generates the minimal unit of the process, that according to the geometry desired, is compatible, and hence, manufacturable.

This thesis is divided into six chapters and a conclusion section. In Chapter I, Background, the topic of manufacturing is addressed, and how a component is determined to be manufacturable or not. It is highlighted that manufacturability has been widely studied for conventional processes, but not for AM, much less in an integral approach, therefore, there is an opportunity for the development of this doctoral thesis considering the material-process-geometry relation.

With the information reported in the Background, the problem is stated in Chapter 2 and, based on this, the hypothesis is proposed, as well as the objectives to be met, the scope and the available resources in the laboratory where this work was developed.

In Chapter 3 the theoretical framework is presented, this chapter contains the information to study the interaction between the material conditions and process parameters, as well as its impact on the manufacturing of parts built by metal additive manufacturing. Additionally, the tools to carry out the study of material-process interaction and manufacturability are presented.

In Chapter 4, the study of material-process is developed. This chapter contains studies by authors who have explored the material characteristics together with manufacturing parameters. Considering this, the concept of processability and its analysis is proposed. Finally, different researches are analysed, with the objective of exploring the concept and analysis proposed.

Once processability is proposed for LPBF-M and explored, the study of manufacturability is developed, in this section, it is summarized the research of complex structures, such as

thin walls and small cylinders using LPBF-M. Afterwards, manufacturability concept is proposed.In this chapter future experimental procedures are proposed to be carried out through a LPBF-M equipment to study processability and manufacturability. Finally, in Conclusion, the results are synthesized from the processability analysis and manufacturability concept carried out.

Chapter 1

Background

1.1 Manufacture and manufacturability

The manufacture is the conversion of raw material into finished products. It needs the application of physical and chemical operations to transform material properties to achieve the product; this requires the usage of machines, tools, energy and labour [3].

Manufacture aims to obtain higher added value in the process, keeping the possible lowest cost. Thus, it is necessary to know if a product is manufacturable or not, and if it is, know how complex it is and how many operations it requires [4].

In order to achieve successful manufacturing, resources must be known, organized, controlled and focused on competitiveness like cost, flexibility, quality, performance and timing. In literature, this is known as Manufacturability and is defined as: *the design characteristics which indicate how difficult or easy the design is from a manufacturing perspective* [4–6].

Through the study of Manufacturability, it has been possible to increase competitiveness, reduce production time and improve the product through the identification and resolution of manufacturing problems [7–9].

Manufacturability studies have been carried out through binary measures (if it can or cannot be built), qualitative (poor, average, good, excellent), abstract quantitative (manu-

facturability index), and time and cost measures; this has been proposed to evaluate conventional processes like machining assemblies, electrical circuit printing, stamping, injection moulding and sheet metal work [7–9].

The study of Manufacturability for conventional processes can be traced to World War II, due to political pressure to have better quality weapons. After this international confrontation, the global incremental competition, and the desire to reduce time and cost, led to increased consideration awareness in manufacturing [7, 8, 10].

The manufacturability study evolved into design methodologies, such as Design for Manufacturing (DfM), where the design product considers the manufacturing process and limits. DfM has the objective of [11]:

- Optimizing all manufacturing functions: fabrication, assembly, manufacture testing, acquisition, shipping, service and repair.
- Ensuring the best cost, quality, reliability, normative compliance, security, purchase time and customer satisfaction.
- Ensuring that manufacturing difficulty does not compromise functionality, style, or product delivery improvement.

Product cost is primarily determined at its planning and design stage; whenever large-scale production starts, only a little can be expected regarding cost improvement, around 80% of manufacturing is committed during the conceptualisation and design phases for any product, this is shown in Figure 1.1, but by the time of production, 95% of the cost is defined, that is why modifying any issue at this stage is too late. For conventional processes, a complex component may require many steps to manufacture, increasing the design and manufacture costs and times [7, 8, 10, 12].

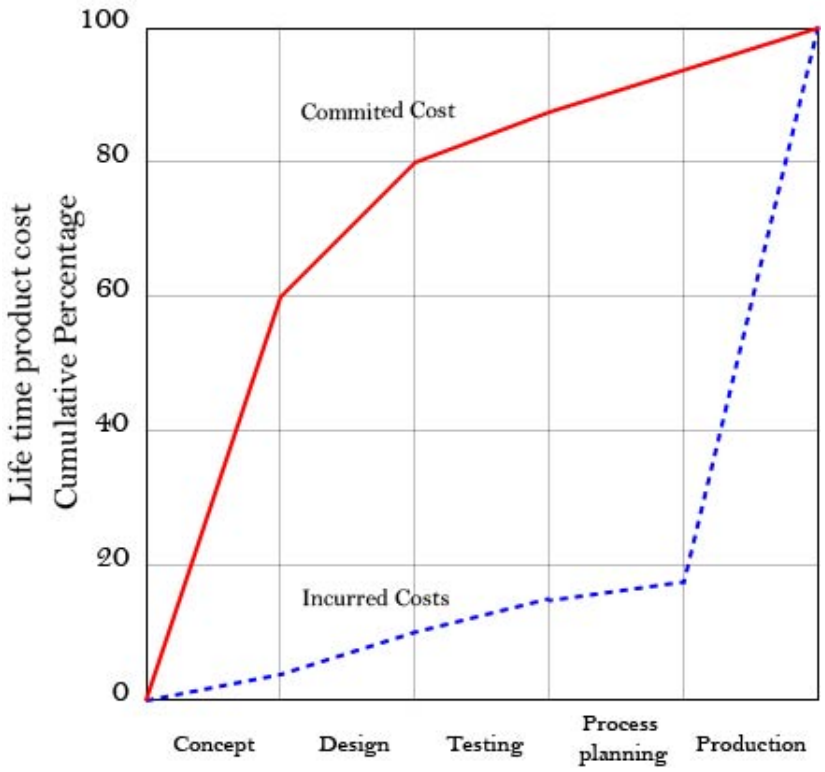

Figure 1.1: Product life cycle [12].

1.2 Additive manufacturing

Building complex designs with Additive Manufacturing (AM) is different, since AM allows for the construction of reticulated structures, components with internal channels, variable layer thickness, undercuts, blind holes, topologically optimized geometries, and custom parts (such as implants and assemblies), all within the same cycle, without the need for tools that might be difficult to achieve with conventional processes. AM is defined as *the process of joining materials, usually layer by layer, to make a three-dimensional object, contrary to the subtractive manufacturing process* [13–16].

AM is known as additive fabrication, free-form fabrication, and rapid manufacturing; the term 3D printing has been indistinctly used to refer to AM, nonetheless it is pretty different, as 3D printing is associated with low-cost machines and low manufacturing capacity. In

contrast, additive manufacturing encompasses different processes, including 3D printing [17, 18].

To profit from AM advantages, shifting from design for a conventional process to Design for Additive Manufacturing (DfAM), is necessary. DfAM is defined as *a set of methods and tools that help the designer take into account the specificity of AM (technological, geometrical, etc.) during the design stage* [19].

The ASTM529000 Standard presents a proposal where AM is classified into seven processes depending on the form of the raw material and the way layers are deposited; this is also considered in ASTM F2792. The seven processes of this classification are briefly presented textually and technologies associated with them are mentioned too [19, 20]:

- **Binder jetting** *"Additive manufacturing process in which a liquid bonding agent is selectively deposited to join powder materials".*

  In this process material, that is available in the form of powder is capable of being processed; typically Al-based, Cu-based, Fe-based, Ni-Based, and Co-based alloys have been used with this technology, but also ceramics such as glass, sand and graphite. Binder jetting uses two materials, the metal or ceramic material (material of which the part is made of) and binder material (which glues the metal/ceramic). The parts built by Binder jetting require several post process steps like curing, depowdering, sintering, infiltration, annealing and finishing [21–23].

- **Direct energy deposition** *"An AM process in which focused thermal energy is used to fuse materials by melting as they are being deposited".*

  Direct energy deposition (DED) operates similarly to welding, with the difference that it uses a nozzle that is not fixed to a certain axis and moves in various directions, depositing material in a workspace while a thermal energy source targets and melts the powder. This process is utilized to create near-net-shape components and repair and add extra material to existing components. This method has been used with

ceramics and polymers but is widely used with metal powder. Laser Engineering Net Shape (LENS) and Electron Beam Additive Manufacturing (EBAM) are DED-process technology. [24–27].

- **Material extrusion** *"AM process in which material is selectively dispensed through a nozzle or orifice".*

  The material extrusion process involves a continuous extrusion of material filaments, viscous inks and polymer pellets through an orifice or nozzle that deposits the material onto a build platform where it is solidified. Fused deposition modelling (FDM), fused filament fabrication (FFF), 3D dispensing, and 3D bioplotter are technologies categorized in this process [28–30].

- **Material jetting** *"AM process in which droplets of build material are selectively deposited".*

  Material jetting (MJ) uses piezo-printing heads to drop photopolymers in liquid form in a selected area and then cure them with ultraviolet light to produce a layer. At the same time, a roller rectifies the thickness of each layer. The same head almost simultaneously solves the material jetting, curation and rectifying. As this process generates 3D parts based on ink jetting technology, it is commonly referred to as 3D inkjet printing or direct inkjet printing [31–33]. MJ equipment can incorporate different colours and materials, allowing localized tuning of material performance [30, 34]. MJ includes Polyjet, NanoParticle Jetting (NPJ) and Drop on Demand (DOD) technologies.

- **Vat photopolymerization** *"An AM process in which liquid photopolymer in a vat is selectively cured by light-activated polymerization".*

  Four types, based on the light source and projection onto the photopolymerizable material, categorize this process. These are: Stereolithography (SLA), Digital Light Processing (DLP), Continuous Digital Light Processing (CDLP) and two-photon polymerization (TPP) [35].

- **Sheet lamination** *"AM process in which sheets of material are bonded to form an object".*

  In this AM process, 3D objects are created by bonding trimmed sheets, it combines both additive and subtractive technologies. Material used in this process includes paper, wood, ceramics and metals. Sheet lamination is classified in two categories: Laminated Object Manufacturing (LOM) and Ultrasonic Consolidation (UC) [36–39].

- **Powder bed fusion** *"An AM process in which thermal energy selectively fuses regions of a powder bed".*

  This process includes the following: Selective Laser Sintering (SLS), Direct Metal Laser Sintering/Selective Laser Melting (DMLS/SLM), Multi Jet Fusion (MJF) and Electron Beam Melting (EBM). Powder Bed Fusion process will be described deeper in the next subsection.

1.2.1 Powder Bed Fusion (PBF)

In PBF, powder is spread on top of a bed through a wiper or scrapper, material is processed with a source of energy that selectively melts the powder, once a layer is finished, a new powder layer is deposited on top of the previous process layer in order to be bonded together, a generic diagram of PBF is shown in Figure 1.2 [40].

Polymers, ceramics and metallic alloys are processed with PBF. In the case of polymers, the powder is used as a support material to build overhang features. For metallic alloys, support structures are necessary for cantilever areas of less than 45 degrees above the platform [41–43].

Selective Laser Melting (SLM) process metallic powder material in an inert gas, with a spot size of 50 to 100 µm, laser power (P) from 50–400 W, scan velocity v of 200–2500 mm/s, layer thickness l_{t} from 30–60 µm and powder material size of 20–40 µm. In Electron Beam Melting (EBM), an electron beam is used to process only metallic alloys; for this process, the

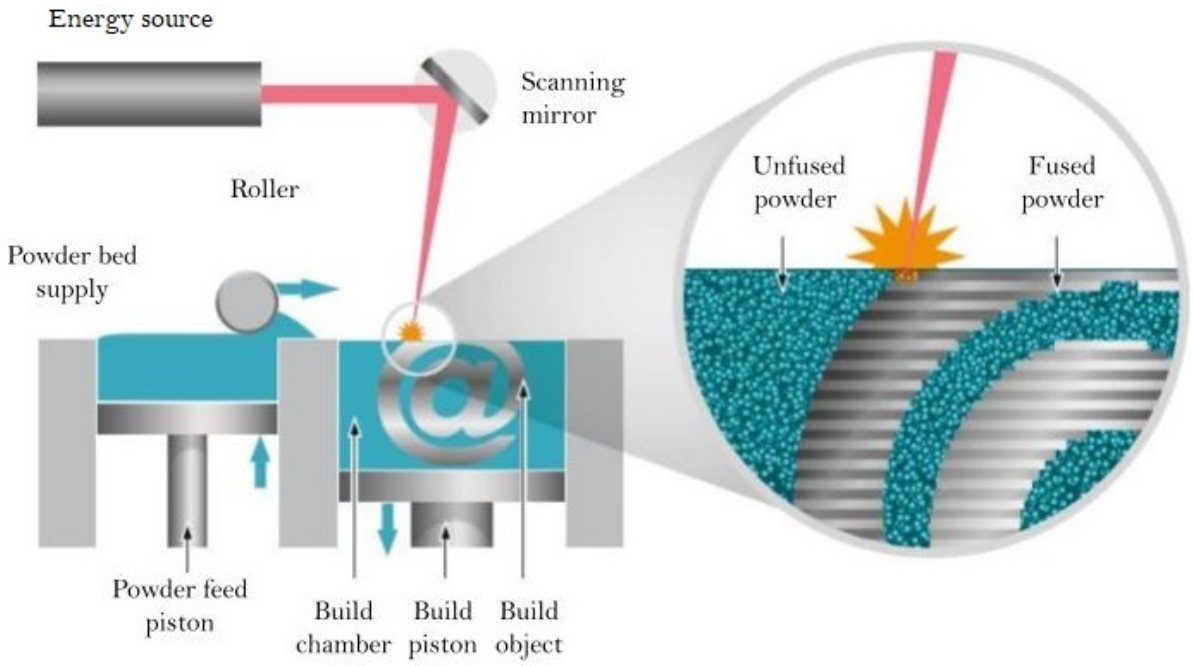

Figure 1.2: General diagram for Powder Bed Fusion process [40].

powder must be an electrical conductor to free the absorbed electrons. EBM is carried out in a vacuum chamber to prevent oxidation and avoid powder contamination. Electron beam size for EBM usually is in the range of 120–140 µm, P above 3000 W, v from 3000–4200 mm/s, l_t from 50–200 µm and powder material size of 40–100 µm [44–49].

1.2.2 Laser Powder Bed Fusion Metal (LPBF-M)

PBF for metallic alloys, is found in literature research with different denominations, some of them are: SLM (Selective Laser Melting), DMLS (Direct Metal Laser Sintering), Laser-Cusing, DMLM (Direct Metal Laser Melting) and LMF (Laser Metal Fusion). It is worth mentioning that each of these denominations depends on the commercial brand names but is still the same process. In this document, LPBF-M (Laser Powder Bed Fusion Metal) is

the term that will be used to refer to the SLM process since, specifically, it refers to the processing using a laser powder bed fusion for metallic alloys. [50, 51].

In LPBF-M, the metallic powder is spread in a bed by a roller or a blade to be selectively melted by a micrometric laser spot (σ_{spot}) with a power P that moves with a certain velocity v. Laser melts the powder according to 2D sections via user-defined toolpaths. When the Laser irradiates the powder, a liquid volume (named the melting pool) is created, which in the first layer is bonded with the platform, named the substrate. The melting pool is adjacently bonded with another melt pool separated a distance, denominated as hatch distance (h_d). When the 2D section is processed, the bed lowers a distance named layer thickness (l_t) and new powder is spread on top of the previously processed layer, and the laser process it, bonding both layers. The process is repeated until all the layers of the part are completed [49, 52, 53].

1.2.3 LPBF-M applications in industry

A global market of metallic components built through LPBF-M has grown, mainly in areas such as: automotive, aerospace, medical and advanced technologies. The main manufacturers of LPBF-M systems are: EOS GmbH (Germany); Concept Laser (GE Additive, Germany); SLM Solutions Group AG (Germany); 3D Systems Inc. (USA); Renishaw plc. (United Kingdom); TRUMPF GmbH +Co. KG (Germany) and V VELO3D (USA) [51]

As a consequence of the cost-benefit relationship and its flexibility in the production of a component, results obtained from-building with LPBF-M are directly incorporated into the development of the production chain. This has led to LPBF-M being used more and more in industry, given that machine sales grew considerably from 2013 to 2018 from 500 to 2200 machines. The number of equipment sold is an indicator of the growth of LPBF-M in the industry, as is observed in Figure 1.4

According to Wohlers Report data of 2020, the four main fields in which the LPBF-M

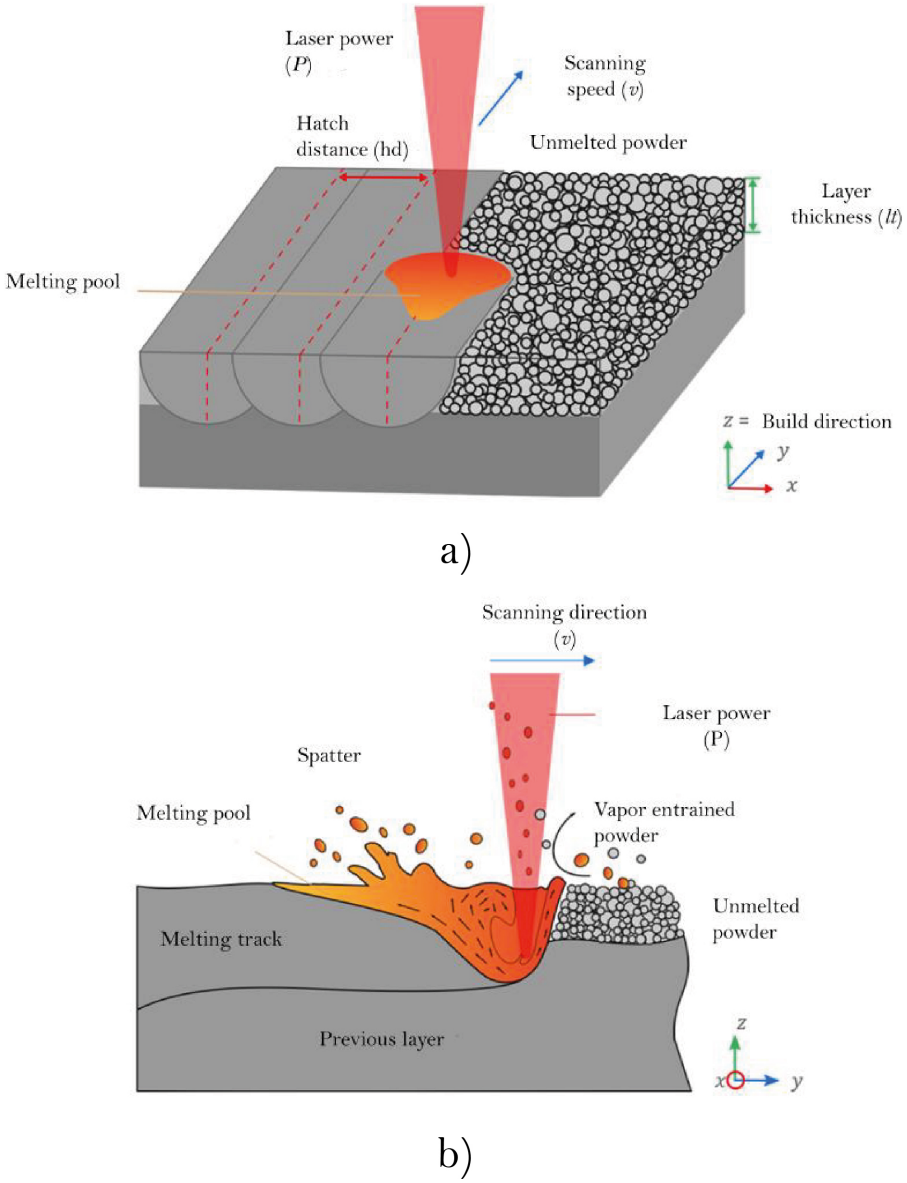

Figure 1.3: Powder Bed Fusion a) Schematics of LPBF-M process parameters b) Formation of spatter particles [53]

process is applied in the industry were: automotive (16.4%), consumer goods and appliances (15.4%), aerospace (14.7%) and medical/dental (13.9%) [54].

An example of LPBF-M aerospace application has been that of GE Aviation which has produced fuel nozzles for its LEAP since 2013, augmenting the life of the fuel delivery system,

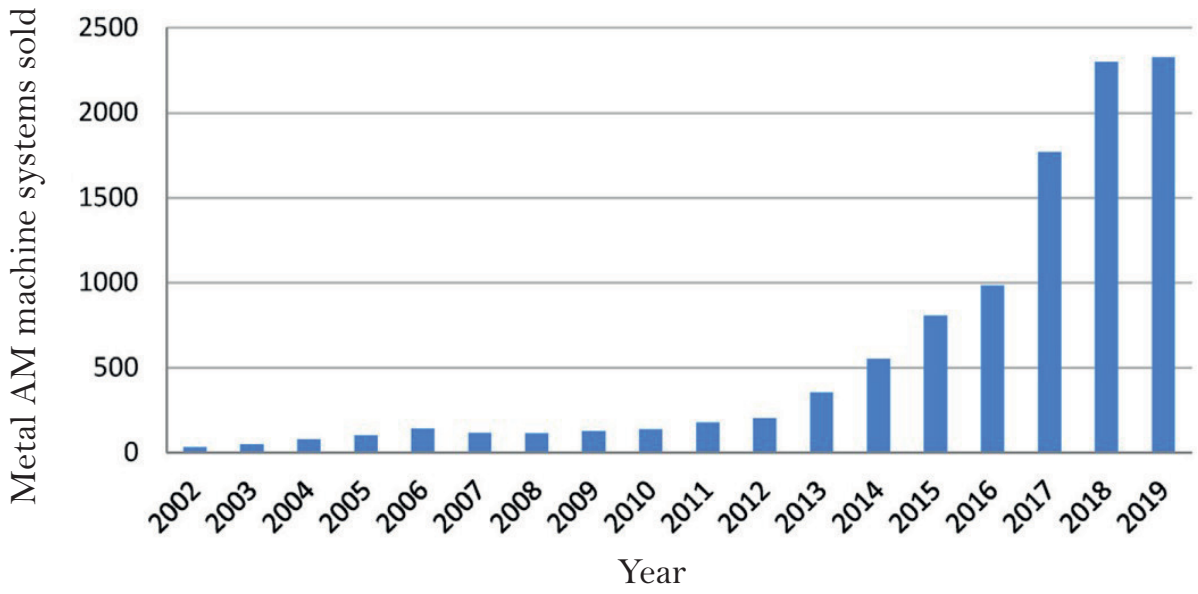

Figure 1.4: Machine solds from 2002-2019 [51]

reducing weight 25% and the part numbers from 20 to 1 (Figure 1.5a) [55, 56].

The aerospace company specialized in subsystems, HPS, designed and built an antenna with a diameter of 300 mm using LPBF-M with Ti6Al4V in collaboration with, IWS, Fraunhofer Institute for Material and Beam Technology and ESA, European Space Agency [57], by using LPBF-M, production time was reduced by 50%, as well as weight and number of individual components compared to the original design (Figure 1.5b).

In the case of an automotive application, the enterprise Bugatti designed and built a Ti6Al4V brake calliper in collaboration with IAPT (Fraunhofer Research Institution for Additive Manufacturing Technologies). This component is considered one of the most extensive parts built with LPBF-M, as it is 41 cm long, 21 cm wide, 13.6 cm high and weighs of 2.9 kg, it achieved a 40% weight reduction in comparison to a conventional aluminium brake calliper [58]. Betatype developed another automotive application; this company manufactured headlight components, where heat skunks were required, using the freedom of LPBF-M of layering several components in the same build cycle, achieving 384 components, thus reducing the price from 30£ to 3£, plus lead time construction went from 440 to 30 hours (Figure

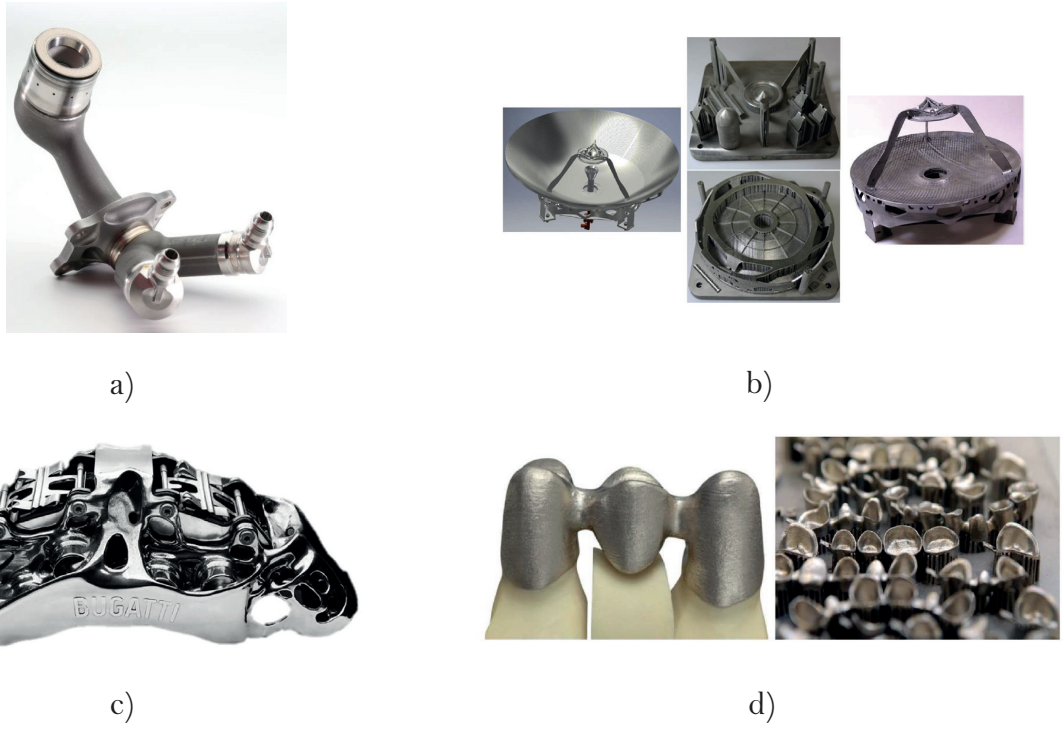

a) b)

c) d)

Figure 1.5: LPBF-M components in industry a) Fuel nozzles of Motor LEAP for GE aviation b) HPS antenna made of Ti6Al4V c) Bugatti break calliper d) BEGO dental implants.

1.5c).

In general, AM has advantages in building custom parts for patients in the medical sector. BEGO, is a German company specializing in dental implants in which customers send the STL file of their teeth scan; after analysis, the company manufactures the necessary teeth crowns with LPBF-M in 48 hours, and the implant's precision is 20 µm [59].

1.3 Lightweight structures

The idea of using porous structures in engineering comes from nature, which has modified the structure of living beings to place material only where it is necessary, obtaining light but resistant elements. Examples in nature of porous structures are, honeycombs, bird beaks and wood [60, 61].

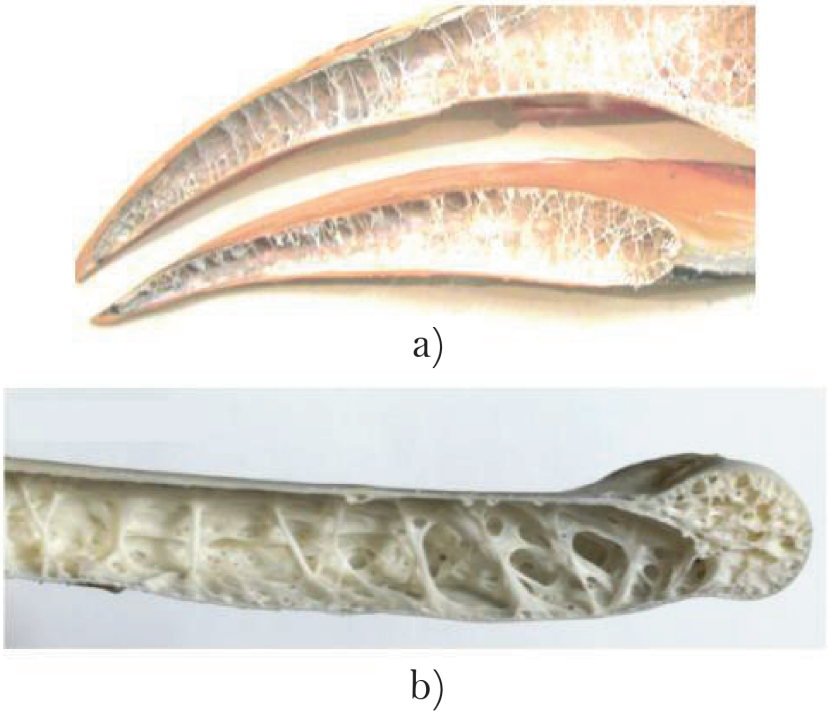

Figure 1.6: Example of a lightweight structures found in nature, which provide strength and rigidity at minimum density a) Bird beak b) Bird wing bone [62].

For a lightweight structure constructed artificially to be considered as such its porosity is required to be greater than 70% and that it is made by means of interconnected porous arrangements through struts or walls (unit cell), in literature it is agreed that a unit cell is in the range from 0.1 to 10.0 [mm]. Depending on the architecture, porous structures are classified in two configurations: random (stochastic) and periodic (non-stochastic) [63, 64].

Stochastic structures are foam with an open and closed cell unit; their uncontrolled distribution is mainly due to the type of manufacturing with which it is built, which is based on the injection of gasses such as oxygen, nitrogen and argon or in addition to agents that release the gas when the foam melts, these gasses generate bubbles within the foam, forming the porous structure [63, 64].

On the other hand, periodic structures are characterized by an organization of controlled cell units, which are periodically distributed in three dimensions; this type of structure is

configured by 2D or 3D arrangements that are uniformly distributed in space; some examples are: Voronoi, Triply periodic minimal surface (TPMS), lattices and custom 3D structures. Periodic, as much as random structures, are shown in Figure 1.7 [63, 64].

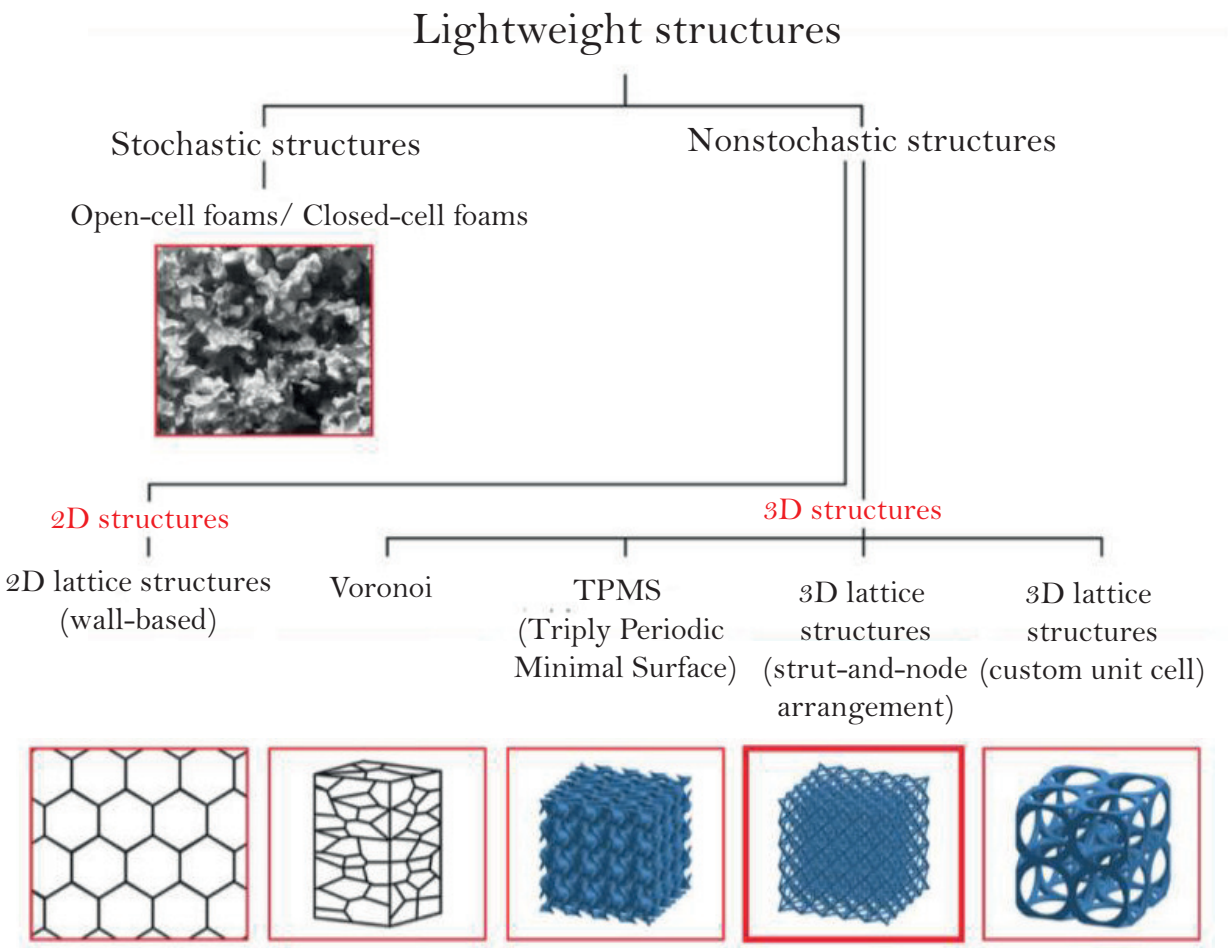

Figure 1.7: Lightweight structures classification according to literature [64].

The word "lattice", comes from french "latte" and describes a structure that contains crossed and attached strips of wood or metal, with spaces between them and in the shape of squares or diamonds [65]; in engineering, it refers to a structure with elements interconnected by nodes that form spaces distributed three dimensionally [66].

Lattice structures possess a certain combination of geometric characteristics, mechanical properties and physical properties [67], which make them suitable for applications such as

thermal insulators, shock and vibration absorbers, sound absorbers, medical implants and overhang supports [68].

One of the main advantages of AM is that it allows for the construction of complex structures such as porous structures that, with traditional processes, would imply more manufacturing steps. However, there are limitations in AM when it comes to building smalls features or structures, because not all designs can be manufactured with AM technology (Mayerhofer et al. 2021) since components such as reticulated structures push the capabilities of AM process to the limit [69, 70].

1.4 Manufacturability for Additive Manufacturing

Manufacturability for AM, specifically for LPBF-M, has been studied from a binary approach, that is, if it can be built or not, and if it is possible to manufacture; manufacturability is visually evaluated with the purpose of identifying how many defects the component has [10]. Zhang et al. 2020 [10] states that manufacturability depends on the relationship between three areas: material, process and geometry, as it is shown in Figure 1.8. This relationship has an impact not only on its manufacturability but also on the porosity, roughness and mechanical performance [10, 71, 72].

Manufacturing lightweight structures through AM is different than manufacturing solid continuous components; its construction with LPBF-M is associated with certain complexity since, as it is a layer-by-laser process, the strut formations obey different mechanisms; for example, for horizontal stratus, they are formed by one or more melt tracks, for vertical melt pools they are formed through melt pools one on top of the other, while for diagonally oriented struts, these are formed through one or more melt pools that are offset to the layers, this offset depends on the angle at which the desired strut is oriented [73].

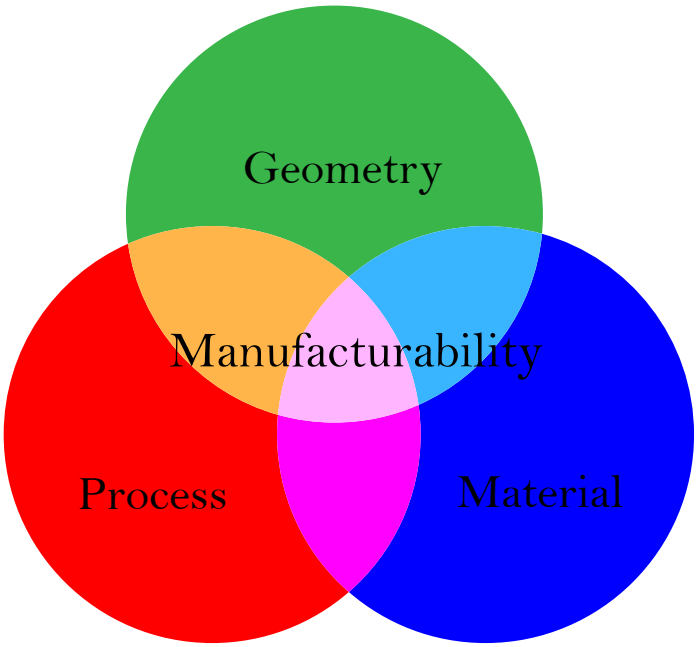

Figure 1.8: Manufacturability approach for AM proposed by Zhang et al 2020. [10]

1.5 Variability in the LPBF-M process

Manufacturability depends on three aspects, but knowing if a part is manufacturable is not quite easy. Selection of manufacturing parameters is not intuitive, especially because LPBF-M is a multi-variable process and does not follow linear behaviour. If a parameter is modified, it has repercussions on final characteristics, including the microstructure, relative density, dimensional precision, surface finish and mechanical performance [74].

In the case of porous structures, it is reported in the literature that a successfully manufactured geometry for LPBF-M equipment may not be successful if the standard process parameters are modified, nor if these standard process parameters are transferred into a different LPBF-M brand machine [10, 75]. Figure 1.10 exemplifies how, with equipment "a", it is possible to manufacture a cubic lattice structure successfully, but not with equipment "b"; manufacturing parameters are shown for both equiments.

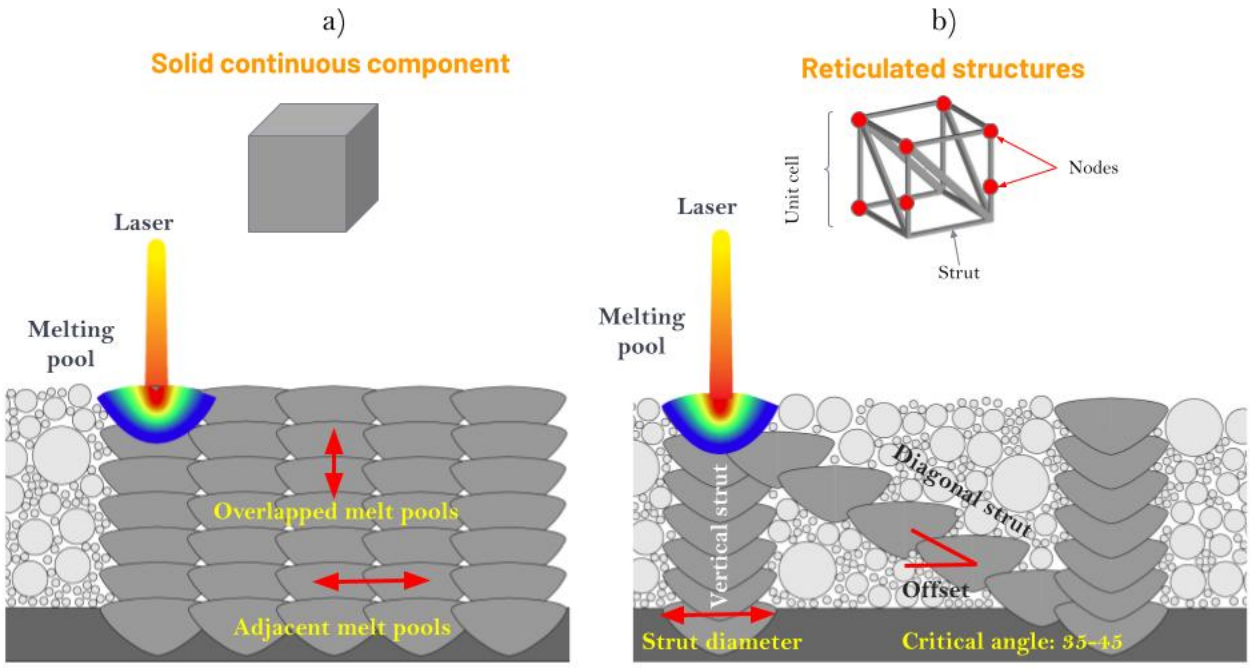

Figure 1.9: Manufacturing differences between continuous solid components and reticulated structures a) Solid continuous component, in this case melting pools are close vertically and adjacently b) Lightweight structure formed by melt pool tracks on top of each other (vertical) and melt pools that are offset to layer (diagonal) (Adapted from [10]).

According to Yadroitsau et al. and Bertoli et al. [76, 77], there are around 130 different parameters involved in the LPBF-M process. However, the laser power (P), scanning speed (v), hatch distance (h_d), and layer thickness (l_t) are the most studied parameters. To establish a relationship between these parameters, scaling laws have been used; such is the case of energy density (ED), which involves P, v, h_d and l_t. Energy density could be expressed in three ways: volumetric (E_v), superficial (E_s) and linear (E_l) equations 1.1-1.3. Deposited energy, another scaling law, has also been used, which is the power divided by the square root of the speed, as indicated by equation (1.4) [76–79].

$$ED_v = \frac{P}{v \cdot l_t \cdot h_d} \tag{1.1}$$

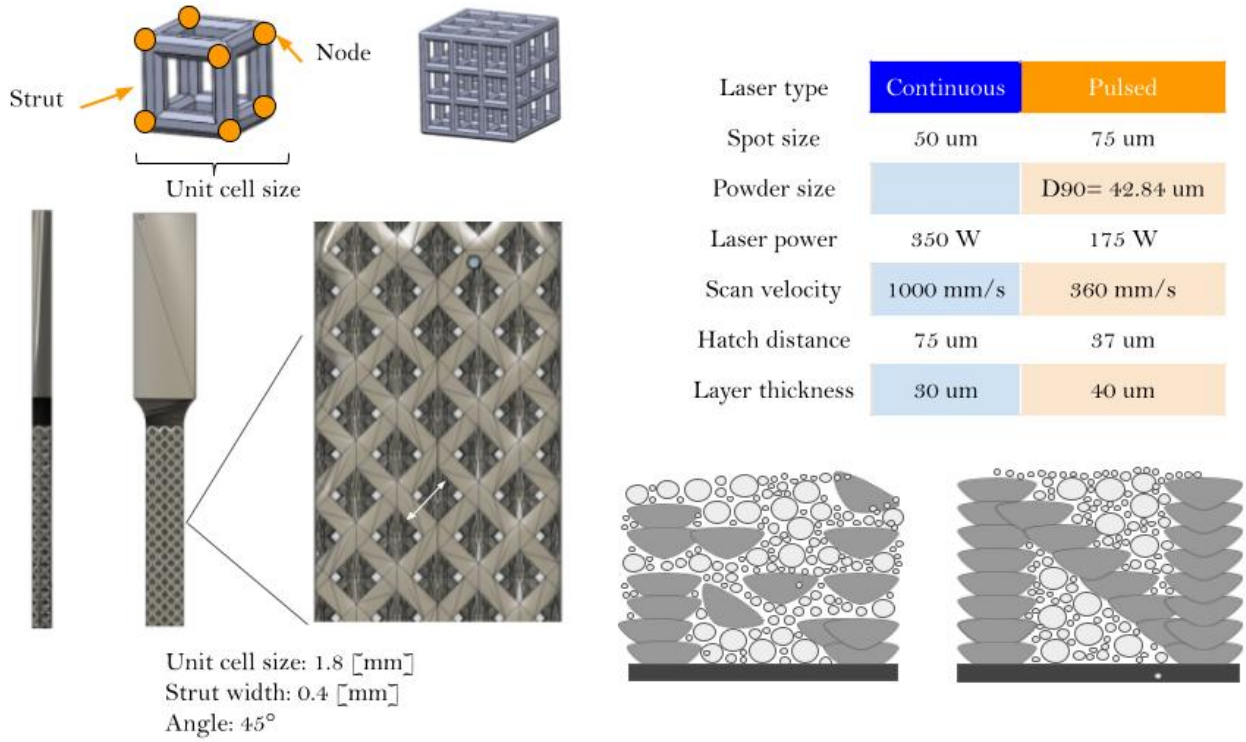

Figure 1.10: Manufacturability of a lightweight construction component comparison between two different LPBF-M machines.

$$ED_{\mathrm{s}} = \frac{P}{v \cdot l_{\mathrm{t}}} \tag{1.2}$$

$$ED_{\mathrm{l}} = \frac{P}{v} \tag{1.3}$$

$$E_{\mathrm{dep}} = \frac{P}{\sqrt{v}} \tag{1.4}$$

An energy density disadvantage ED is that the value could be the result from different combinations of P and v, achieving different component properties and performance. For example, using an h_d of 100 µm and a v of 50 mm/s results in the same linear volumetric E_v value as an h_d of 50 µm and a v of 100 mm/s, with P and l_t being constant. Another

disadvantage is that a suitable ED value is not replicated in other equipment, therefore identifying when defects (such as porosity) appear is very difficult; ED law has been widely studied but also questioned, since it does not consider the material characteristics [76, 80].

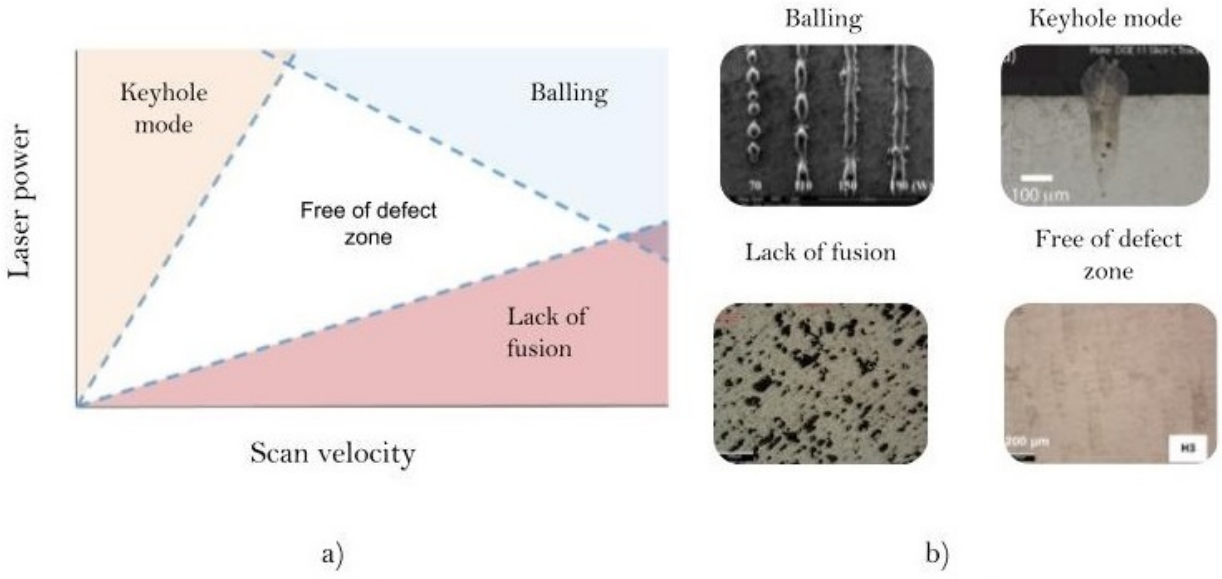

Figure 1.11: a) Construction window P vs v b) Defects in LPBF-M according to construction window (Adapted from [81]).

ED has been helpful in developing construction windows (under particular material conditions), as shown in Figure 1.11. In said construction window, different regions of defect-free operation are identified, defect zones are presented depending on the parameters used: balling effect, which occurs at high laser power and high speed; keyhole defect, which occurs due to high power and low speed; and lack of fusion, due to a low power [81].

When material conditions change, manufacturing parameters identified as suitable for one material-specific condition are not necessarily transferable to another; this has caused not only the lack of transferability of manufacturing parameters, but also variability in the mechanical performance of parts built by LPBF-M with different equipment that use different process parameters and material conditions. This is represented in Figure 1.12, in which the results of three authors that studied 316 stainless steel alloy are compared. It

is worth mentioning that different manufacturing parameters are used, obtaining different energy density values; even so, relative densities higher than 98% are obtained but with different mechanical performances [82–84].

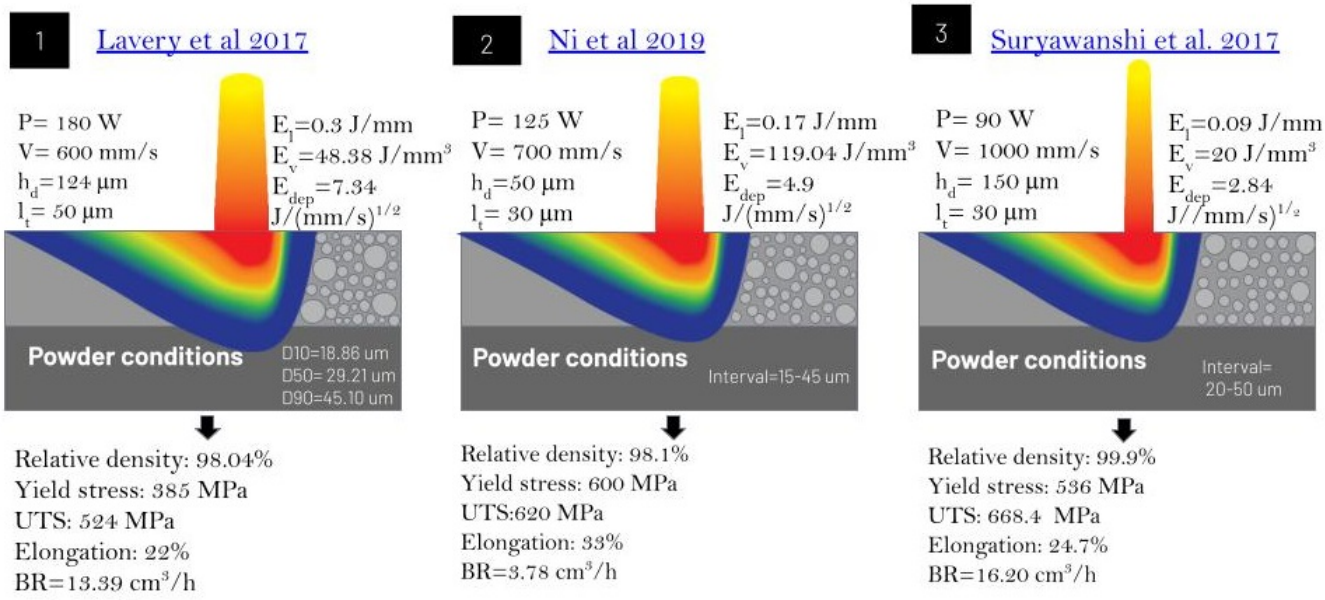

Figure 1.12: Variability in LPBF-M

Chapter 2

Problem statement

The use of different process parameters combined with different powder characteristics and LPBF-M equipment has caused variability in the components built with this technology in terms of mechanical performance, productivity, surface finish, dimensional accuracy, microstructure and hardness; this has caused that the process to not meet standardization requirements that conventional manufacturing processes currently have. Furthermore, it is unknown if a complex geometry, such as a lightweight structure, will be successfully manufacturable when using different process parameters and powder characteristics. It is also identified that, although the material-process-geometry relationship is proposed in literature research (as the one proposed by Zhang et al. [10]), defining manufacturability quantitatively is still required, since this author's approach allows knowing which items depend on manufacturability, but fails to explain whether a part is manufacturable or not, and if the construction success can be predicted. To define manufacturability for LPBF-M, it is proposed to be studied using the material-process relationship that defines the fundamental unit of the LPBF-M process, that, if compatible with the geometry desired, will make a successfully manufacturable component [71, 85]. Based on this, the following hypothesis is proposed.

2.1 Hypothesis

It is acknowledged that the the manufacturability of components constructed with LPBF-M depends on three aspects: material conditions, process parameters, and the desired geometry to build. Therefore, it is hypothesized that the study of the relationship between the material characteristics and process will determine whether a geometrical characteristic is manufacturable.

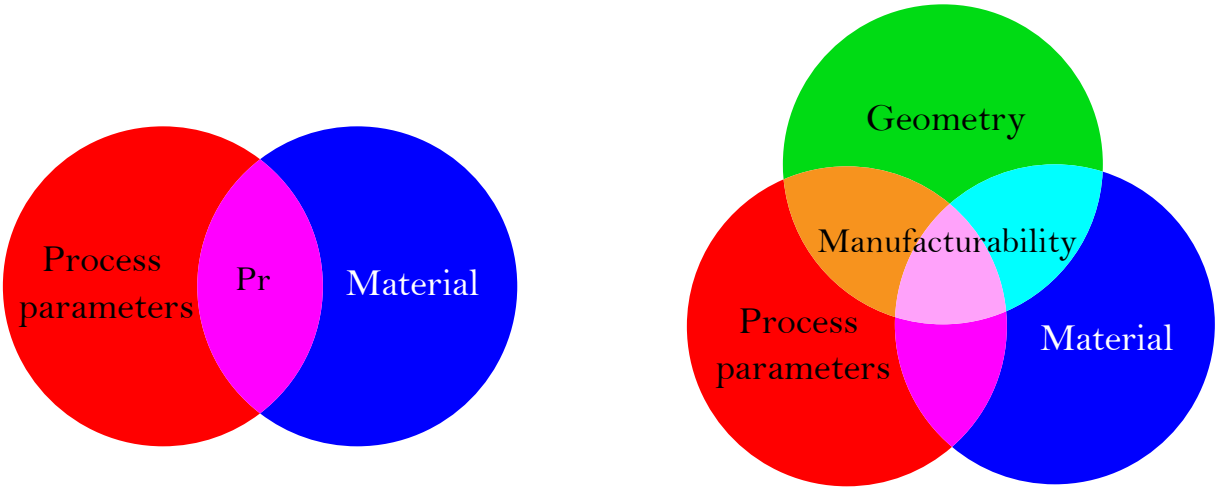

Figure 2.1: Study of manufacturability from the material-process interaction.

2.2 Main objective

The objective of this research is to identify the limits of geometrical structures from the interplay between material characteristics and the process parameters within LPBF-M. This involves a meticulous exploration of the distinctive features of the material and the spectrum of process parameters inherent in any given machine. Within this study, the objective encompasses different alloys, revealing the potential of its applicability.

2.2.1 Specific objectives

- To study the material-process interaction and the main parameters that affect the LPBF-M process, in order to propose an integral approach, defined here as processability concept for LPBF-M, as well as an quantitative approach.
- Based on processability study, complement the concept of manufacturability for LPBF-M through the study of a fundamental unit, as a result of material-process interaction.

2.3 Goals

- Identify the effects of the powder material characteristics and process parameters on the melting pool and temperature.
- Obtain a quantitative measure of processability based on the interaction of the material (properties, size and morphology of powder alloy) and process parameters (laser power, scan speed, layer thickness and hatch distance).
- Study the relationship between material characteristics and process parameters and its compatibility with geometry to determine whether a structure is manufacturable.

2.4 Available resources

This doctoral research was developed in the facilities of the National Laboratory of Additive and Digital Manufacturing (MADiT), at its headquarters in the Institute of Applied Sciences and Technology (ICAT) located in Universidad Nacional Autónoma de México (UNAM), the following equipment was used:

- Electromechanical universal testing machine: Shimadzu AGS-X-50kN
- CT scanner: Nikon XT H225

- LPBF-M manufacturing machine Prox320

Chapter 3

Theoretical framework

3.1 Thermal phenomena involved in the LPBF-M process

The LPBF-M process uses a laser as a source of energy; when the powder is irradiated by the laser, physical phenomena are involved in the process. The absorbed energy is transformed into thermal energy, suddenly increasing the temperature until a maximum is reached. When the temperature is greater than the melting point (T_m) powder particles become a "wet" volume, typically known as melting pool, if the temperature continues to increase, the pool reaches a suitable width and depth to join with other pools, either horizontally or vertically. If power is high enough, the boiling point (T_b) can be reached [51]. Melt pool formation is a highly dynamic and complicated process that involves the four states of matter: solid, liquid, vapour, and plasma. It also includes vaporization of material, recoil, convection, vapour impact, multiple reflection and absorption, melt pool osculations, protrusion and instabilities [86–89].

In the LPBF-M process, heating and cooling rates are in the order of 10^3-10^8 K/s, the thermal gradient is within 10^6–10^8 and its word mentioning that it is beneath the Gaussian profile beam centre; temperatures can be hundreds of kelvins above evaporation powder

temperature [90–95].

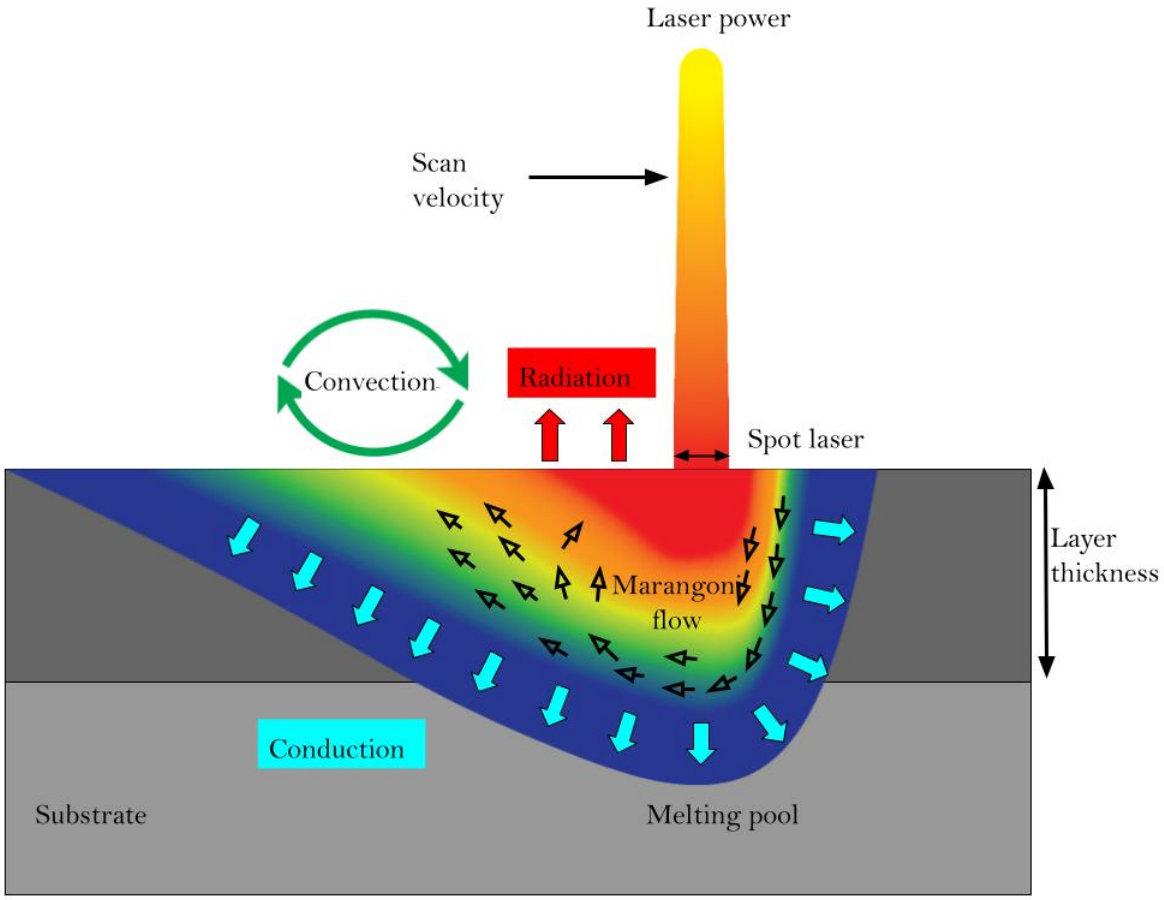

Figure 3.1: Diagram of the melt pool generated in the LPBF-M process adapted from [96].

Th melting pool has dynamic movement within; the heat transferred in the material generates temperature gradients in the liquid pool, which leads to fluid moving inside the pool; this is known as the Marangoni effect. Depending on process parameters, the quantity and quality of the liquid formed influences the level of densification and the continuity of the track due to rheological behaviour occurring during melt pool generation [97–99]; this is measured by dynamic viscosity μ:

$$\mu = \frac{15}{16}\sqrt{\frac{m}{k_{\mathrm{b}}\,T}}\,\gamma \tag{3.1}$$

Where m is the atomic mass, k_b is the Boltzmann constant, T is the melt pool temperature, and γ is the surface tension of the metal part. As can be seen, the temperature considerably influences melted part viscosity, modifying its wettability and liquid solid rheological properties.

From Equation 3.1, it is possible to observe that a high temperature decreases dynamic viscosity in the melt pool, a low μ with a long liquid life produced by high-temperature increases instability of the melt pool and the Marangoni effect. Marangoni number (M_{an}) is given by:

$$M_{\text{an}} = \frac{\Delta_\sigma \, L}{\mu \, \nu_\kappa} \tag{3.2}$$

Where Δ_σ is the Marangoni surface tensión difference, L is the length of the free surface, and ν_κ is dynamic viscosity. High temperatures produced by high powers form intense currents caused by the decrease of μ, raising the thermal capillarity magnitude force and, therefore instability in the melt pool, compensating for the low energy on the surface of the melt material.

As the laser moves across the platform and leaves the molten volume, the melt pool begins to cool and eventually solidifies, forming a single track, which is the fundamental unit of bonding in LPBF-M; the bonding of adjacent single tracks creates a single layer and a 3D object is formed from a sequence of layers [51, 77, 98, 100].

3.2 Process parameters

ISO/ASTM 52900:2015 defines process parameters as: *a set of operating parameters and system settings used during a single build cycle* [51]. For LPBF-M, it is crucial to select process parameters according to material alloy since each one requires different inputs of energy due to thermal properties and characteristics (absorptivity, powder size distribution, thermal conductivity, diffusivity and heat capacity) if the material is not processed under

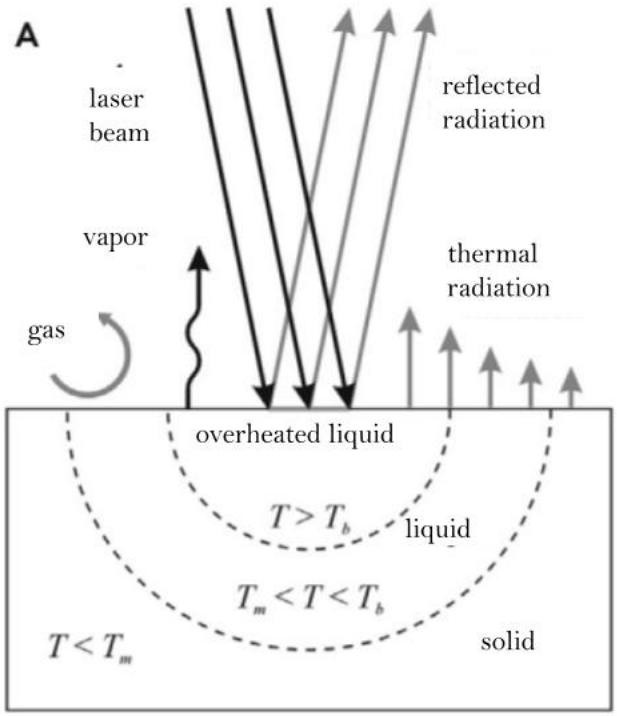

Figure 3.2: Energy transformations due to the interaction of the laser beam with a solid object

proper conditions, the final piece may be porous and not have the required quality [101], that, according to the ISO 9000 standard, is defined as *the degree to which a set of inherent characteristics fulfils requirements.*

For LPBF-M, quality means high relative density, dimensional precision, appropriate microstructure and high repeatability of built parts [51]. According to literature for LPBF-M [76, 77, 102], 130-157 process parameters affect the manufacturing parts. However, the most commonly investigated parameters identified in the literature are laser power (P), scan speed (v), scan strategy (ss), hatch distance (h_d) and layer thickness (l_t).

3.3 LPBF-M defects

It is expected that LPBF-M will have more adoption in industry applications. Thus, the process must meet engineering quality standards; this means that LPBF-M must be free of defects, such as pores, one of the most adverse effects on mechanical performance [103].

LPBF-M offers a significant advantage in building complex components that would be very difficult or impossible to build by conventional methods; it has been reported that the process is affected by factors such as power-scan speed ratio, scan strategy and metallic powder alloy condition (size and morphology) [104]. These factors affect the three types of heat transfer, melting, solidification and, therefore, the evolution of the microstructure, the Marangoni effect and material evaporation. If process parameters and material conditions do not produce an adequate melting pool or if melting mools are not bonded adequately among them, defects will manifest through pores, cracks and impurities [105–108].

In the case of the melting pool, its dimension (depth, width and length) and temperature, will be defined according to material properties and characteristics, as well as the process parameters [109]. Typically, it is desired a "healthy" smooth and continuous melting pool, as the one shown in Figure 3.3. This kind of melting pools are associated with the conduction regime, in which the temperature is above T_m but below the T_b, here, the melting pool cross-section is semicircular (melt pool depth is shorter than or equal to its half-width [110]). Such a "healthy" melting pool bonded with others of the same characteristics, will produce free of defects components when using adequate (h_d) and (l_t) [76, 111].

The following sections describes some defects that occur in the LPBF-M process, including keyhole mode, lack of fusion and balling effect.

3.3.1 Keyhole mode

If the combination of laser power and scan speed exceeds a threshold, it can change from conduction to keyhole mode. In this mode, the energy is sufficient to cause the evaporation

of powder on the surface, producing a dense vapour plume that originates a recoil momentum on the molten material to form a cavity; vapour fails to escape and is trapped within the melting pool [44, 112, 113].

As the name implies, the melting pool takes a keyhole shape, where the cross-section is deeper and narrower than in conduction mode, where the cross-section is considered semi-circular. Keyhole mode is no stranger to other processes in which a laser is used to melt alloys, as it occurs in processes such as laser, electron beam, and plasma arc welding [114].

Bertoli et al. 2017 [76] identified the melting pool depth as a function of the energy density (E_D) scaling law. Nonetheless, E_D does not include the necessary material information to establish the transition between conduction and vaporization.

In order to identify the conduction-vaporization threshold, a model proposed by Kings et al. 2014 [112] has been used; this author based his studies on Han et al. 2011 research [115] welding data, which showed that the information of the melt pool for different alloys and different machines could be represented in a single curve since the relationship between melt pool depth (D) and spot laser diameter is a function of deposited energy ΔH and enthalpy of fusion h_s. According to this model, this relationship is defined as:

$$\frac{\Delta H}{h_s} = \frac{A\,P}{\pi\,h_s\sqrt{D\,v\,\sigma}^3} \tag{3.3}$$

3.3.2 Lack of fusion

Lack of fusion occurs when a melt pool does not bond properly with the previous layer or with adjacent melt pool tracks. This results in discontinuous layers that lead to the creation of pores, decreasing mechanical properties and worsening surface finish. Lack of fusion is associated with low laser power or very high scan speed, also with high l_t that does not allow vertical bonding of melt pools, and h_d if not small enough to avoid gaps [114, 116]. Figure 3.3 illustrates lack of fusion; this defect is located at the bottom of the P-v diagram.

According to Mukherjee et al. 2016 [117], an adequate interlayer bonding for any alloy

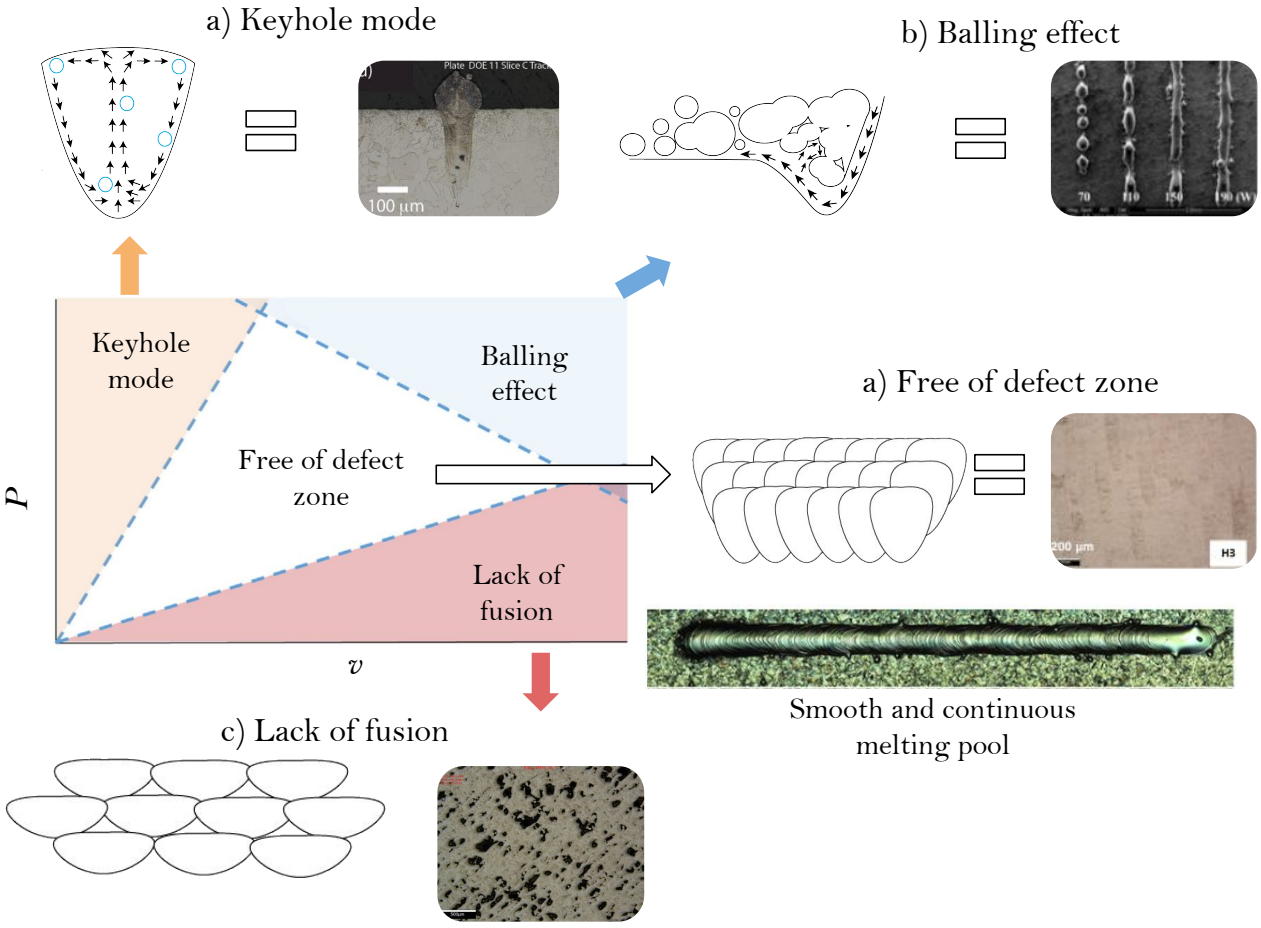

Figure 3.3: Defects in LPBF-M and its relation with melt pool morphology a) Keyhole mode b) Balling effect c) Lack of fusion.

can be analysed by considering a dimensionless index between melt pool depth (D) and l_t, which is recommended to be greater than 1.1. On the other hand, Eskandari et al.2019 [118] proposed a 1.5 ratio. In the case of adjacent pools, Tang et al. 2017 propose that h_d divided by melt pool width W must be less than 1 to guarantee that melt pools are as close as possible to prevent void-formation [119].

3.3.3 Balling effect

The balling effect occurs when a melt pool does not wet a solid part, leading to a discontinuity between the melt pool and the solid substrate, fragmenting the melt pool into solid balls [116].

This effect is mainly produced by a high P in the melt pool, causing the limits of the melt pool to have different conditions than in the centre of the melt pool; this generates pressure differences produced by the Marangoni effect. These balls generated by high power prevent the formation of uniform melt pools, and the distribution of a new fresh powder layer is not uniform either, and can increase roughness and delamination due to poor union between layers, in addition, these "balls" can damage the powder feeder [116, 120, 121].

The intrinsic properties of alloys used in LPBF play an important role when processing material. Typically, alloys have "balanced" properties between melting point, thermal conductivity, surface tension and viscosity. Titanium and stainless steel alloys are typically "easy" alloys to process. They exhibit low thermal conductivity and good melting, surface tension and viscosity values, meaning that melt pool "wetting" is more easily achieved since the heat transfer is uniform. At the same time, copper and aluminium are "difficult" to process.

In the LPBF-M process, it is recommended that the power and speed generate a sufficient temperature to form melting pool, i.e. the fundamental unit, whose dimensions, together with process parameters such as hatch distance and layer thickness, allow suitably bond with the others to avoid defects in certain time. These are the basis to study the material-process interaction (Section 4.1. Once the minimal unit is known, it is proposed the study of manufacturability (Section 4.2)through its compatibility with a complex geometry, such as a wall or an angled strut. Thus, it is important to know characteristics such as melting pool dimensions and temperature. This is carried out through equations to calculate these characteristics which are presented in Section 3.4.

3.4 Analytical equations that define the interaction material-process

With the objective of quantifying the material-process interaction, analytical equations are identified from literature and described, particularly to calculate Temperature (T) and melt pool dimensions.

3.4.1 Temperature

For a Gaussian laser the T at the center of the irradiated powder is given by:

$$T = \frac{\sqrt{2}\,A\,I\,\sigma}{k\,\sqrt{\pi}}\,\tan^{-1}(\sqrt{\frac{2\,\alpha}{v\,\sigma}}) \tag{3.4}$$

Where I is the intensity of the laser and is calculated as:

$$I = \frac{P}{2\,\pi\,\sigma^2} \tag{3.5}$$

A is absorptivity, α is thermal diffusivity and k is thermal conductivity.

3.4.2 Melt pool dimensions

Rosenthal equation has been used to calculate thermal profiles for laser welding [122] however, given its similarities to LPBF-M, it has also been used to obtain thermal profiles in this additive process [119,123]. With this equation it is possible to determine the thermal profiles for a melt pool, the value that defines melt pool dimensions is given by the T that reaches T_m.

$$T = T_0 + \frac{Q_P}{2\,\pi\,R\,k}\,exp[\frac{-v\,(\xi + R))}{2\,\alpha}] \tag{3.6}$$

Where T is the local temperature, T_0 (K) is the temperature inside the machine chamber.

P (W) is laser power, v (m/s) is scan speed, k (W/mK) is thermal conductivity, α is thermal diffusivity, R is defined as $R = \xi^2 + y^2 + z^2$ (m) and is radial distance from the laser position, ξ is the laser distance along its path, y is the distance parallel to the piece and z is the depth below the piece. Tang et al. 2017 and Pistorius et al. 2017 [119, 123] used a simplfied Rosenthal equation to calculate melt pool width (W) and depth (D), this is defined as:

$$D = \frac{1}{2} W \approx \sqrt{\frac{2\,A\,Q}{e\,\pi\,\rho\,C(T\,-T_0)}} \tag{3.7}$$

3.4.3 Build rate

Build rate is a measure of productivity, and it indicates the amount of material melted per unit time. For LPBF-M it involves v, l_t and h_d, it is calculated through the following equation [124, 125]:

$$BR = v \cdot h_d \cdot l_t \tag{3.8}$$

These expressions will be used in Chapter 4 to quantify the material-process interaction. Such expressions consider material properties and simplifies the calculations compared to computing simulations, the results may differ from what actually occur in the process, nonetheless other precise method is welcome to be used.

Chapter 4

Development

4.1 Material-process interaction study

In this section the material-process interaction is studied, it is identified that the components, built by LPBF-M, present variability in terms of mechanical performance, attributed to a range of process parameters such as P, v, l_t and h_d and powder material characteristics employed by each machine brand, which generates different minimum process units that interact differently depending on the material and process used, this variation is holding back the adoption of this technology at THE industrial level.

4.1.1 Previous studies of material-process interaction in LPBF-M in literature

Material-process (M-P) interaction research includes the study between the material characteristics and the process parameters (together or separately) to determine its effects on density, lack of defects, surface quality, microhardness and dimensional accuracy.

Welding metallurgy and technologies, the bases of LPBF-M, has been used to understand the LPBF-M process and to improve it; however, specific differences, such as higher energy and a continuous medium used in welding, make it imprecise to apply in a technique like

LPBF, which uses a discontinuous material powder alloy. Characteristics such as powder size, distribution size and morphology have effects on laser absorptivity, melt pool dynamics and dimensions, cooling rates and defects, which have consequences in the final characteristics of the part such as rugosity, relative density, microstructure and mechanical properties [81].

Mukherjee et al. 2016 [117] proposed the concept of printability as *the ability of an alloy to resist distortion, compositional changes and lack of fusion defects* for powder-based AM processes. This concept could be compared with weldability, defined as *the possibility and easiness of two alloys to be welded* [118].

Sisanth et al. 2017 considered material conditions, process parameters, and efficiency. It is crucial to take into account efficiency in the LPBF-M study, efficiency is one of the most difficult challenges to address [125], as LPBF-M built components are constituted of the micrometrical layer made up of micrometrical bonded melting pools, thus construction time is slow compared with the conventional process.

M-P interaction has been carried out to establish a relationship with densification behaviours, such as defect formation mechanisms, at specific processing parameters [126]. Gu et al. 2019 [85] studied the material-process interaction of the Inconel 718 alloy in terms of the influence of particle size on the flow behaviour of powder with the melting and solidification characteristics for the Inconel 718 alloy. They found that smooth melt pool tracks can be created with a powder size of 25 μm, which avoids defects such as balling.

Engeli et al. 2016 [127] studied the IN738LC alloy with batches of different powder sizes regarding melt pool size, width, porosity and cracking and concluded that the slight changes in composition and size distribution of the powder could strongly affect cracking.

Recently, Balba et al. 2021 [128] studied it in terms of density, surface quality, microhardness and dimensional accuracy with a fine powder (D_{50}=9 µm) batch and a coarse one (D_{50}=40 µm). They identified that, with coarse powder, it is possible to achieve higher densities, lower rugosity, finer microstructures and higher microhardness.

Cosma et al. 2020 [129] analysed stainless steel 315, based on experiments; the author pro-

posed the evaluation of material-process interaction according to the quality of construction: i.e., unstable, relatively unstable and stable processability.

In the research presented previously, the term Processability has been employed to addressed the M-P interaction. Processability is critical for determining the cost and efficiency of any material, from its raw material to the final product of any manufacturing process. It refers to the ease of achievement of the required processing schedules since the more stable and repeatable the process is the more feasible production becomes. Studying processability differs considerably from one material to another given its properties [130, 131]

The industry demands materials that can be processed efficiently and demonstrate outstanding performance. Thus, it is desirable to know if a material is processable and, if it is, in which conditions its use is adequate. Processability determines the efficiency of industrial production and also plays an essential role in the final product [132].

This term has been principally defined for polymers, still,given the importance of having more stable processes and increasing efficiency in the industry, the term processability should be defined for LPBF-M too. Therefore in section 4.1.2 the concept of processability for LPBF-M is presented, as well as its measurement, based on the approach that what defines the performance of the components built by LPBF-M, is the fundamental unit produced by P and v, and how it interacts with others through h_d and l_t.

4.1.2 Processability concept proposal for LPBF-M

Based on studies mentioned in section 4.1.1 a processability LPBF-M definition is proposed as ***the estimated Build Rate resulting from free-of-defect components built, taking into account the geometrical conditions of the powder metallic alloy melting pool resulting from the process parameters***.

The following steps are proposed for quantifying processability:

1. Identify a safe range of temperatures for free-of-defect construction (which must be

between the melting and boiling temperatures).

2. Estimate the temperature that will be reached based on the available machine and the selected process parameters (v and P). This depends on the physicochemical properties of each powder alloy.

3. Estimate the dimensions of the melt pool to propose a suitable hatch distance according W to calculate the BR based on v, l_t and h_d parameters.

4. Identify specifications (such as the mechanical properties, roughness, relative density, etc.) that must be characterised for selected BR values.

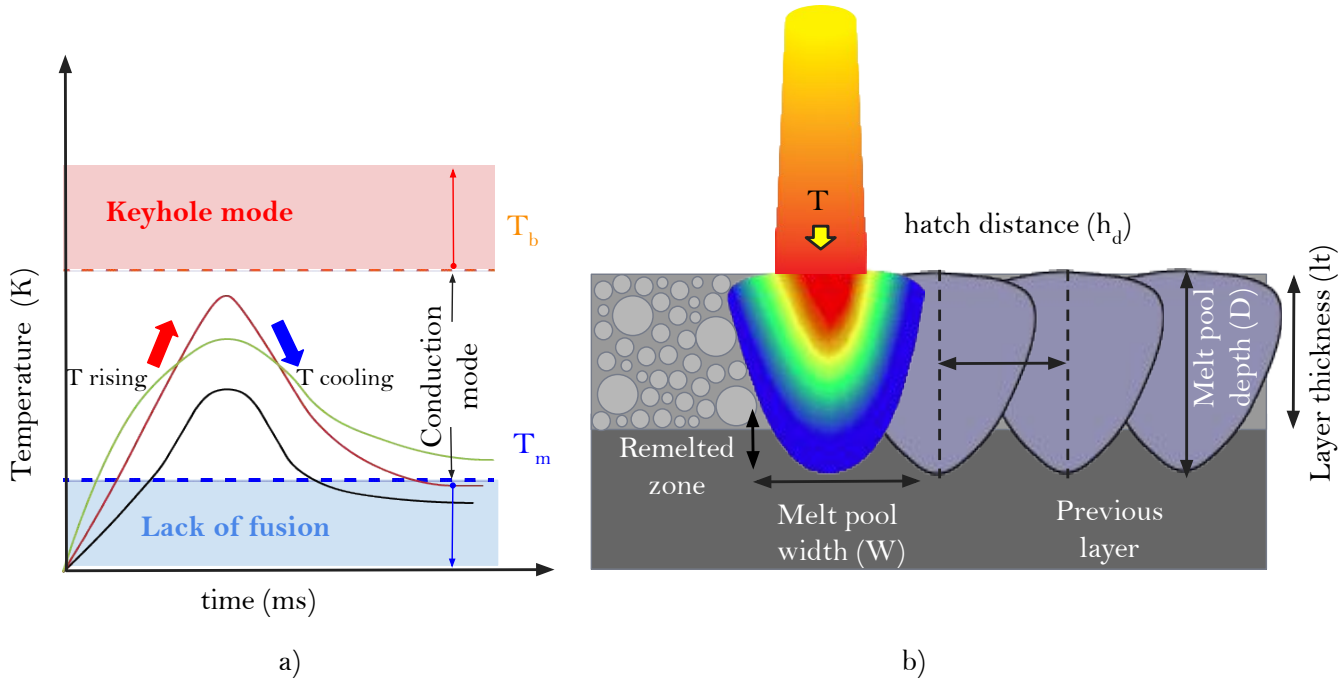

Figure 4.1: Diagram of processability stages and constraints. a) Temperature history according to time, where T conditions are indicated. b) Melting pool formation according to T (T_b and T_m).

LPBF-M starts when the laser spot hits the metal powder, then the temperature (T) rises,

and the melt pool appears when the temperature is higher than the melting temperature (T_{m}). The temperature still rises until it achieves its maximum value according to process parameters (P and v); the maximum temperature should not exceed the boiling temperature (T_{b}). Once the maximum temperature is reached, it begins to cool down, and the melt pool begins to solidify until the temperature of the melt pool falls under the liquidus temperature, this is resumed in Figure 4.1 [133, 134].

$\mathrm{L_t}$ is a process parameter that is chosen according to powder size. More specifically, it is recommended that $\mathrm{l_t}$ is greater than $\mathrm{D_{90}}$, in order to have a suitable distribution of particle powders on the bed whenever powder is placed on it. Nonetheless, it is worth knowing that $\mathrm{l_t}$ is the nominal value that represents the new particle powder spread on the previously solidified layer, but the actual value, known as effective layer thickness ($\mathrm{l_{t\ effective}}$), is larger than $\mathrm{l_t}$ as a consequence of the shrinkage after melting and solidification [135].

Spierings et al. 2011 [136] proposed $\mathrm{l_{t\ effective}}$ to be 60% greater than $\mathrm{l_t}$, because of powder layer density in LPBF which, in this process, is in the range 38–60%. Therefore, the literature suggests that, in order to have an adequate amount of powder particles deposited, the relation between $\mathrm{l_{t\ effective}}$ and $\mathrm{D_{90}}$ should be 1.5 ($\mathrm{l_{t\ effective}/D_{90}} \approx 0.5$) [136, 137].

In the case of melt pool horizontal and vertical attachment, to obtain adequate consolidation with the previous layer, it is recommended in literature research that the melt pool depth (D) is 1.5 times greater than $\mathrm{l_t}$ ($\mathrm{D/l_t} > 1.5$). Meanwhile, to obtain adequate consolidation with adjacent melt tracks, the ratio between $\mathrm{h_d}$ and the melt pool width is recommended to be less than 1 ($\mathrm{h_d/W} < 1$); this means closer melt pools that may avoid inter-track porosities [117–119].

Based on the concept proposed for processability, the steps for quantifying it, and the equations introduced in the previous section, processability plots are generated. These charts show the relationship between T and BR, and indicate the limits defined by the metallic alloy powder. The potential processing region is highlighted in cyan Figure 4.2. The value of T (which is plotted vs. BR for different values of P and v) should be greater than Tm

but lower than Tb, for fixed values of lt and hd.

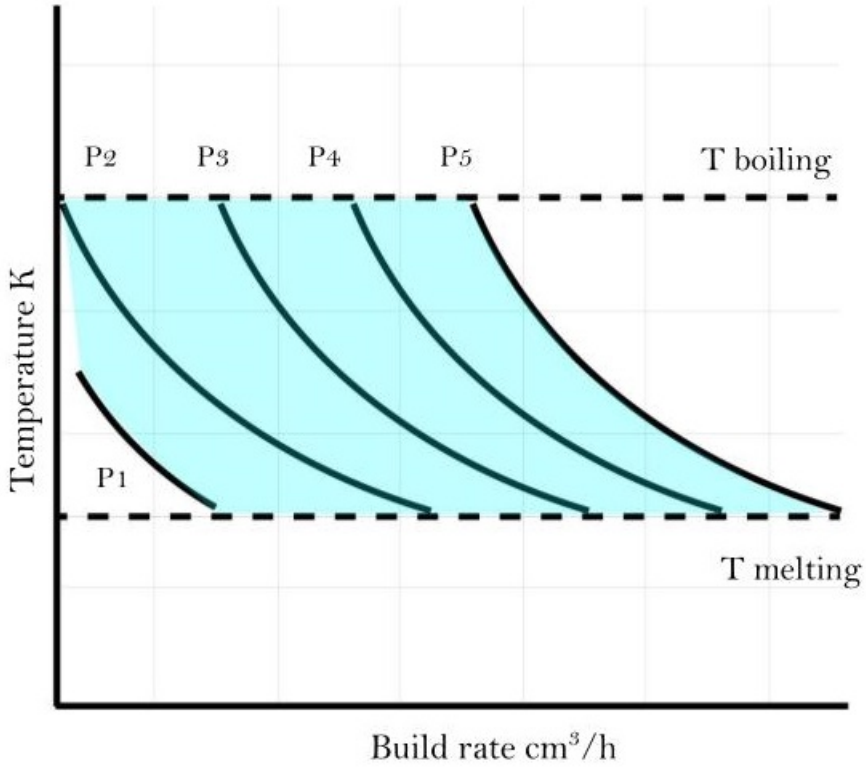

Figure 4.2: Potential processability diagram with differing laser power.

4.1.3 Processability analysis

With the aim of exploring the processability analysis proposed on this thesis, data taken from literature was analysed with different alloys. First, the implications to relative density as a consequence of increasing BR was studied using different P, v and h_{d} for stainless steal 17-4 PH. Notwithstanding, it is important to verify the effects of BR on mechanical performance. For this, a second analysis was carried out comparing processability with different mechanical tests, such as, Tensile strength, Microhardness, Relative density, Flexural strength, Torsional strength, and Wear rate for stainless steel 316.

4.1.3.1 Processability and its effects on relative density

Reported data from Ozsoy et al. 2021 [138] was analysed. This author studied 17-4 PH alloy under different P, v and h_{d}.

From processability analysis and according to process parameters and powder characteristics of the alloy used, it was verified that temperature reached the melting point and that it did not exceed the boiling point, the melt pool ratios $\mathrm{D/l_t}$ and $\mathrm{h_d/W}$ were estimated. Build rate (BR) was plotted according to T, showing that there is a wide processability region where the parameters, in combination with powder characteristics of the alloy, make it suitable to produce parts above 99% of relative density.

Materials and methods

Renishaw AM400 machine, with a construction volume of 250 x 250 x 300 mm, and a Yb-fiber laser with a maximum power of P=400 W, λ=1064 nm and a σ=70 μm. Construction was carried out under an argon atmosphere with leftover oxygen of 100 ppm in the build chamber. The 17-4 PH stainless steel had a powder size distribution of $\mathrm{D_{10}}$=17 μm, $\mathrm{D_{50}}$=33 μm, and $\mathrm{D_{90}}$=48 μm. The alloy properties used in this study for 17-4 PH are indicated in Table 4.1

Table 4.1: 17-4 PH stainless steel properties

Material property	value
Absorptivity (A)	0.35 %
Melting temperature ($\mathrm{T_m}$)	1677 K
Boiling temperature ($\mathrm{T_b}$)	3375 K
Density (ρ)	7750 kg/m^3
Thermal conductivity (k)	22.6 W/mK
Thermal diffusivity (α)	0.000045 m^2/s
Heat capacity (C)	460 W/mK

Analysis and results

Table 4.2: Process parameters used by Ozcoy et al. 2021

Sample	BR	P	v	hd	LED	T	D/lt	hd/W	Density
	cm3/h	W	mm/s	μ	J/mm	K	%	%	%
H7	7.11	200	940.17	70	0.21	1990.28	1.99	0.59	99.88
H4	9.19	200	1216.22	70	0.16	1766.37	1.75	0.67	99.49
H13	9.86	275	1304.35	70	0.21	2350.41	1.98	0.59	99.61
H10	12.6	275	1666.67	70	0.16	2093.14	1.75	0.66	99.03
H16	18.08	275	2391.3	70	0.12	1760.39	1.46	0.80	99.39
H19	12.6	350	1666.67	70	0.21	2664.00	1.98	0.59	99.71
H25	16.31	350	2156.86	70	0.16	2354.75	1.74	0.67	99.21
H22	22.68	350	3000.00	70	0.12	2007.32	1.48	0.79	99.24
H5	7.11	200	731.71	90	0.27	2230.37	2.26	0.66	99.51
H2	9.19	200	945.95	90	0.21	1984.69	1.99	0.76	99.31
H11	9.86	275	1014.49	90	0.27	2642.41	2.25	0.67	99.43
H26	12.43	350	1279.07	90	0.27	3019.04	2.26	0.66	99.45
H17	12.73	275	1309.52	90	0.21	2346.04	1.98	0.76	99.4
H8	13.04	200	1341.46	90	0.15	1686.99	1.67	0.90	99.75
H23	16.2	350	1666.67	90	0.21	2664.00	1.98	0.76	99.41
H14	17.85	275	1836.73	90	0.15	1998.36	1.67	0.90	99.48
H20	22.68	350	2333.33	90	0.15	2267.2	1.67	0.90	99.58
H3	7.11	200	598.29	110	0.33	2439.11	2.50	0.73	99.66
H9	9.20	200	774.65	110	0.26	2173.82	2.20	0.84	99.78
H18	9.83	275	827.07	110	0.33	2901.65	2.49	0.74	99.57
H24	12.43	350	1046.51	110	0.33	3315.08	2.50	0.73	99.45
H15	12.73	275	1071.43	110	0.26	2576.46	2.19	0.84	99.66
H21	16.31	350	1372.55	110	0.25	2920.56	2.18	0.84	99.59
H27	22.93	350	1929.82	110	0.18	2483.9	1.84	1.00	99.15

In Table 4.2, data is sorted with different h_d (70, 90 and 110 μm) only components that achieved more than 99% relative density were analysed, since parts densities above this relative density are accepted as successful in literature [139–141]. All samples met $T_m < T < T_b$, as well as D/l_t and h_d/W ratios.

Then the processability chart was plotted; this is shown in Figure 4.3. The suitable processing region is indicated in cyan color; different process parameters of h_d, T_m and T_b used by this author are also indicated using the color yellow.

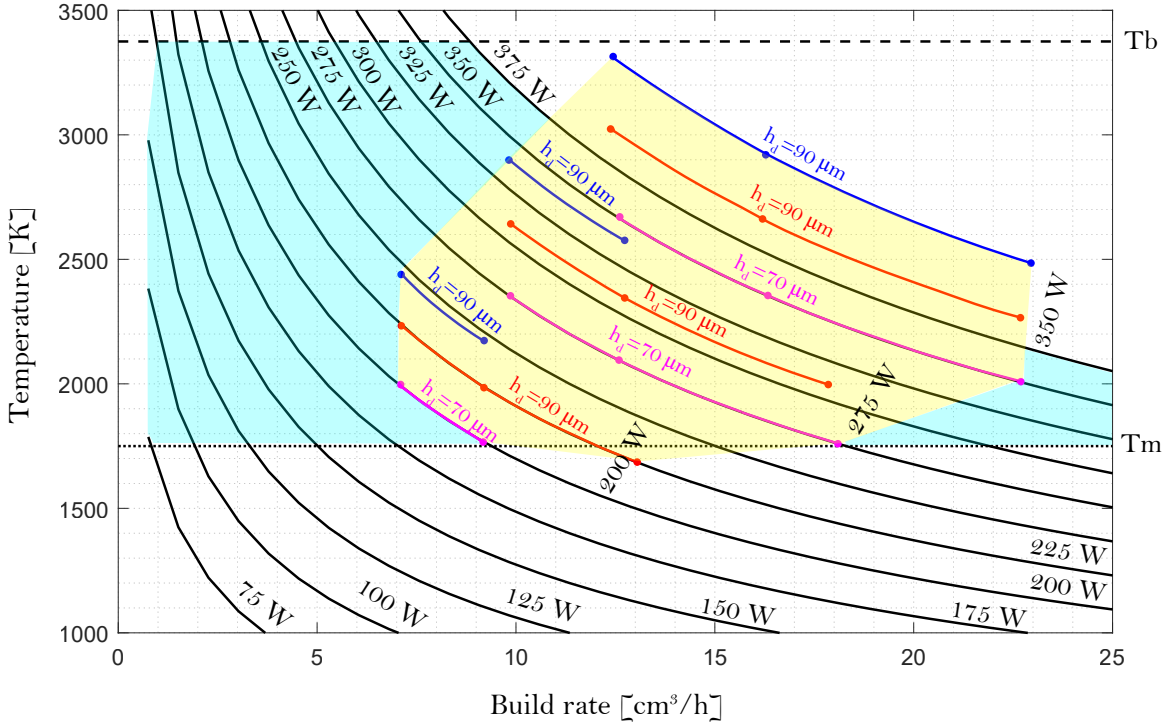

Figure 4.3: Processability chart. The suitable processability region is indicated by the color cyan, meanwhile the processes employed in the study is yellow

For h_d/W, lower ratios than 1 indicate wider attachment distances between melt pools; this value result in higher density, for example, samples H7 and H19. For the D/l_t ratio, every sample in Table 4.2 achieves more than 1.5. The magnitude of this ratio is not fully defined in the literature, but a high deep-layer thickness ratio should lead to a keyhole mode that occurs at a temperature higher than T_b.

As it is shown in 4.3, there is a wide option of combinations for P, v and h_d that achieve T_m and avoid T_b, based on this, the user may choose "healthy" ratios in order to increase BR, for example, low h_d values (70 μm) allow closer melt pools and high h_d (110 μm) separate the pools but allow for an increment of BR.

Relative density was used as a criterion to evaluate processability. It is possible to find

high BRs, up to 22 cm^3/h (as shown in Table 4.2 for H22, H20 and H27) without compromising relative density, i.e., without going below 99%. On the other hand, Table 1 samples H7, H5 and H3 had relative densities above 99.5%, but their BRs were barely above 7 cm^3/h. A previous analysis of processability, with only v, h_d and l_t as the processing parameters, provide an estimate of the BR, energy used and the basis to select which process parameters are adequate to increase productivity without compromising additional criteria such as relative density.

4.1.4 Processability and mechanical implications

An experimental data set, taken from literature [142], was used in order to apply the concept of processability proposed in this work, as well as its effects on mechanical performance. It is identified in literature that the LPBF-M process achieves relative densities up to 99% through different combinations of P, v and h_d, but mechanical performance differ.

Materials and methods

Multiple samples manufactured at different P and v conditions were constructed in discontinuous laser LPFB-M Renishaw AM250 with a laser spot (σ_{spot}) of 70 μm and wavelength of λ=1064 nm. Construction was carried out under an argon atmosphere with leftover oxygen of 100 ppm in the build chamber. Samples were processed with five levels of laser power (120, 140, 160, 180 and 200 W) and three different exposure times (et) of 60, 70 and 80μs, process parameters such as hatch distance (h_d) of 110 μm, point distance p_d of 60 μm, of 50 μm, and meander scan strategy were used. v is calculated as v= pd/et ratio. With v(1-3), BRs were calculated and indicated in Table 4.3.l_t The alloy properties used in this study for SS 316 to realize the processability analysis are indicated on Table 4.4.

Processability results are plotted in Figure 4.4. In this figure, two regions of processability are shown depending on the parameters used. The processability of process parameters

Table 4.3: Process parameters used by zhu et al. 2019

Sample	P	v	LED	BR	T	D	W	D/lt	hd/W
	W	mm/s	J/mm	cm3/h	K	μ	μ	%	%
1	120	1000	0.120	19.80	1584.63	44.73	89.47	0.895	1.229
2	140	1000	0.140	19.80	1848.73	48.32	96.64	0.966	1.138
3	160	1000	0.160	19.80	2112.84	51.65	103.31	1.033	1.065
4	180	1000	0.180	19.80	2376.94	54.79	109.58	1.096	1.004
5	200	1000	0.200	19.80	2641.05	57.75	115.50	1.155	0.952
6	120	857.14	0.140	16.97	1702.60	48.32	96.64	0.966	1.138
7	140	857.14	0.163	16.97	1986.37	52.19	104.38	1.044	1.054
8	160	857.14	0.187	16.97	2270.14	55.79	111.59	1.116	0.986
9	180	857.14	0.210	16.97	2553.91	59.18	118.35	1.184	0.929
10	200	857.14	0.233	16.97	2837.67	62.38	124.76	1.248	0.882
11	120	750	0.160	14.85	1810.73	51.65	103.31	1.033	1.065
12	140	750	0.187	14.85	2112.51	55.79	111.59	1.116	0.986
13	160	750	0.213	14.85	2414.30	59.65	119.29	1.193	0.922
14	180	750	0.240	14.85	2716.09	63.26	126.53	1.265	0.869
15	200	750	0.267	14.85	3017.88	66.69	133.37	1.334	0.825

used by Zhu et al. 2019 [142] are plotted in magenta. Meanwhile, in cyan, the potential processability region is illustrated.

Powders were spherical in the range from 15 to 45 m. Processability plots were carried out based on T and compared with BR according to the process parameters mentioned in this study. Zhu et al. 2019 reported six different mechanical performances: relative density, hardness, tensile strength, flexural strength, torsional strength and wear rate. The results of these mechanical performances were plotted with T and compared to BR. According to process parameters, processability calculations are presented in Table 4.3,as BR and T. Additionally, melt pool dimension estimations and ratios D/l_t and h_d/W are presented.

Analysis and results

The mechanical properties achieved are presented as a function of T in Figures 4.5 and

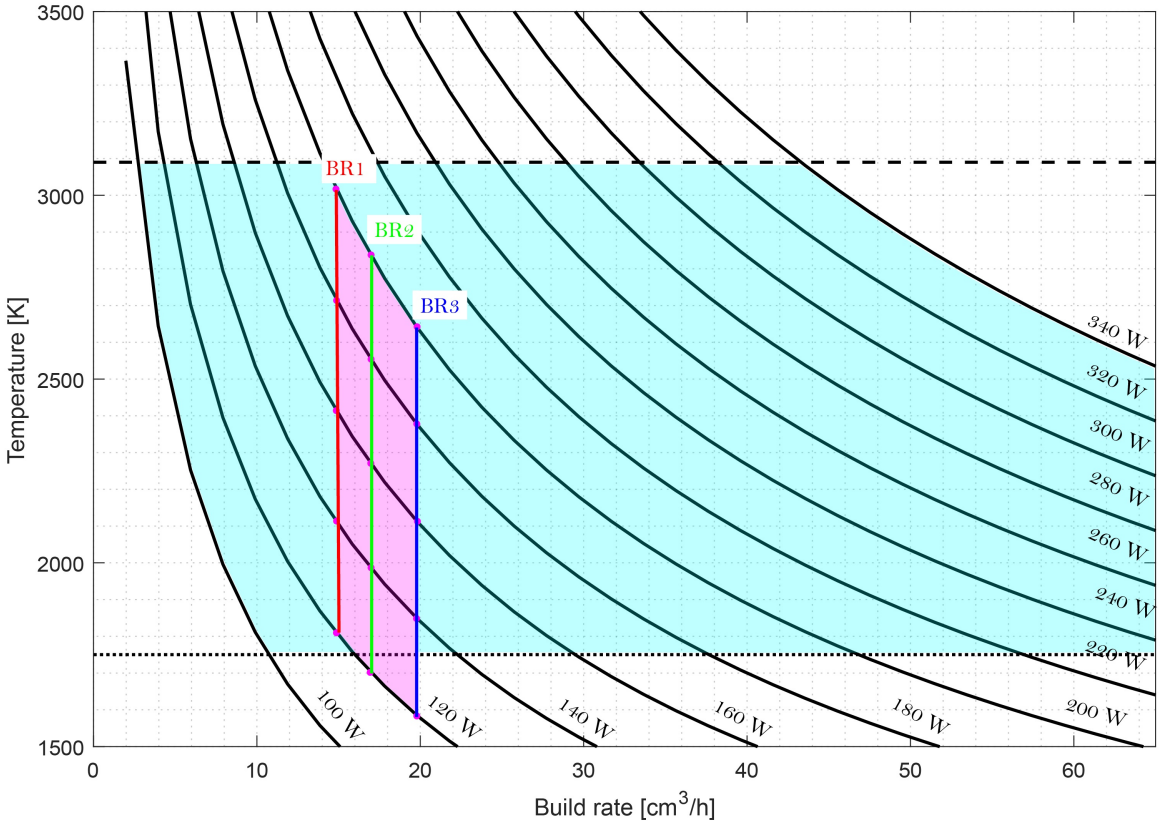

Figure 4.4: Processability stages and constraints diagram.

4.6, at three different BR values (BR_1=14.85 cm^3/h, BR_2=16.97 cm^3/h, BR_3=19.80 cm^3/h. It can be seen from the figure that the performance in terms of the relative density, torsional strength, hardness, and wear rate improves as T increases, for each value of BR evaluated. The tensile strength and flexural strength behaviour reach a maximum value (at around 55% and 75% of the T_b and T_m difference), but decrease as the boiling temperature is approached.

The highest tensile strength is observed to be achieved with BR_3 (the coldest and fastest BR of the three). BR_1 and BR_2 operate with higher T than BR_3; tensile strength diminishes as T_b is approached. The literature shows that boiling temperature is not recommended in the LPBF-M process, as this generates keyhole mode and increases porosity in the component [143].

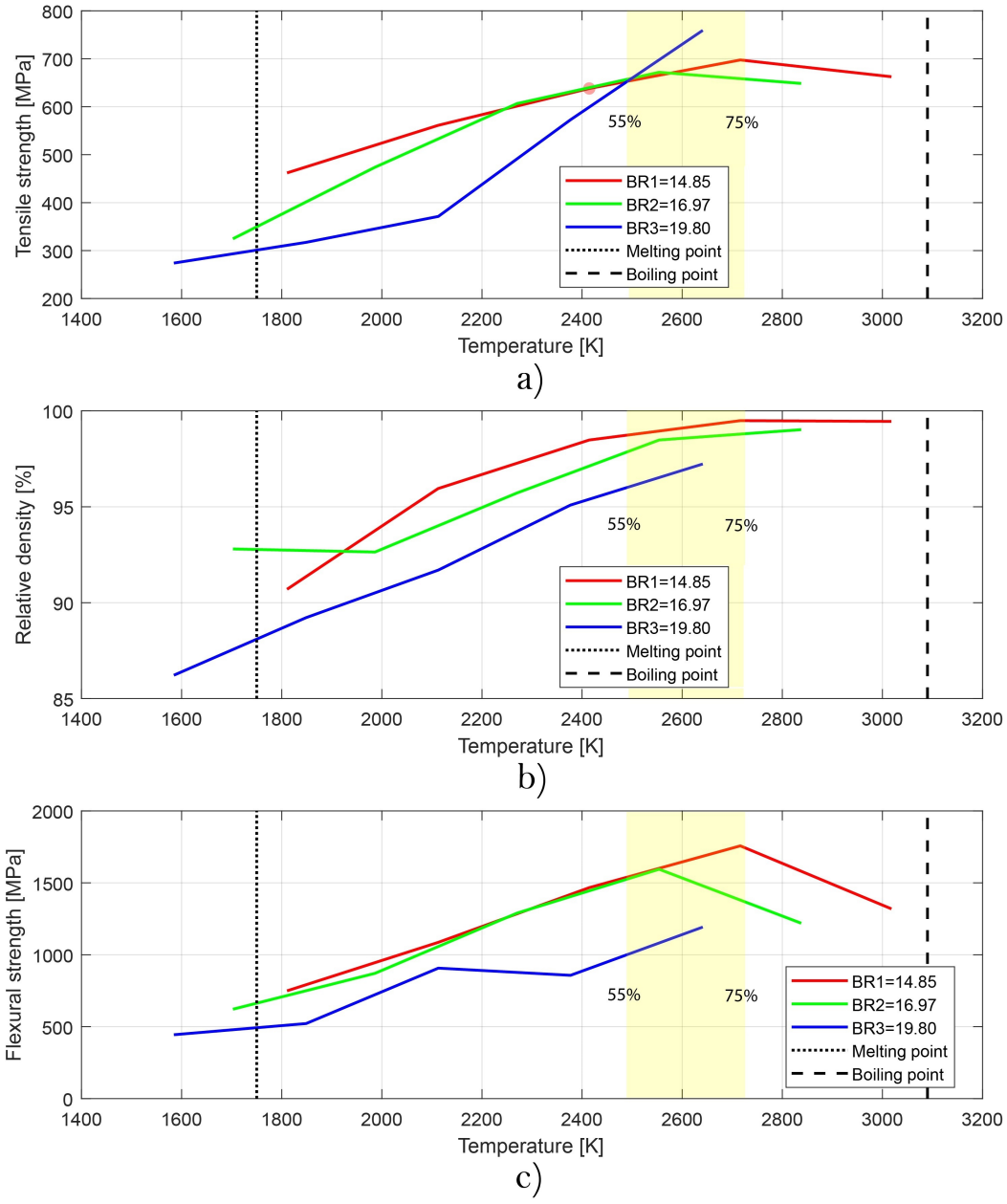

Figure 4.5: Mechanical performance behavior as a function of T and compared to BR. T convergence is indicated in the color cyan.

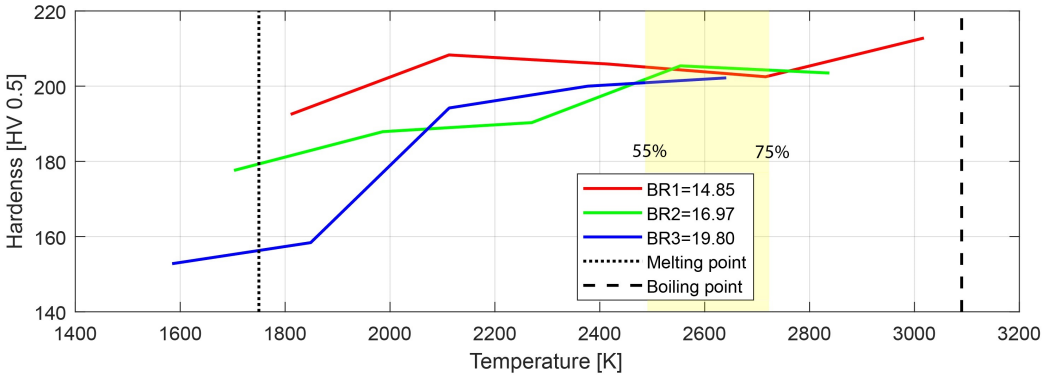

d)

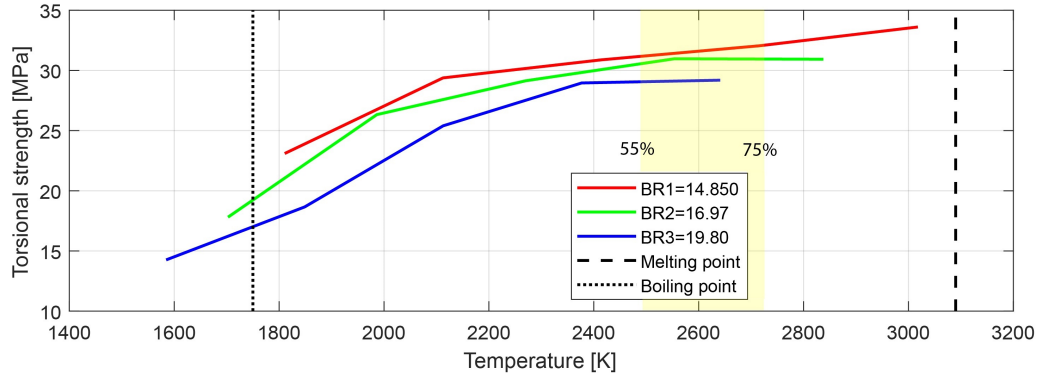

e)

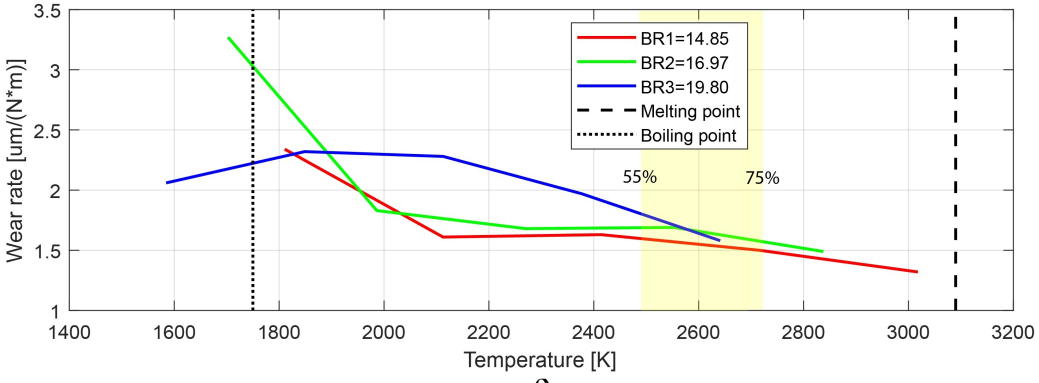

f)

Figure 4.6: Mechanical performance behavior as a function of T and compared to BR. It is indicated on Tensile strength plot convergence T with color cyan.

The Figure 4.5 illustrates that the highest relative density is attained when BR1 and BR2 are at their hottest near Tb. However, this does not correspond to higher tensile strength values. Excessive energy increases the thermal gradient and then promotes cracking [144, 145]. Niendorf et al. [144] showed that for SS316 with a high power (HP) of 1000 W, ductility was improved compared to components built at a low power (LP) of 400 W. However, the properties, such as the ultimate tensile strength, were reduced due to the crystallographic textured columnar grain produced by high P. Montero et al. [145] conducted similar experiments and considered rotation angles between layers of 0°, 45° and 90°. With this scanning strategy, their results showed that the mechanical performance of components built at low P was superior to those built at higher P values regarding elongation, tensile strength, yield strength and hardness.

Table 4.4: 316 stainless steel properties

Material property	value
Absorptivity (A)	0.35 %
Melting temperature (T_m)	1678 K
Boiling temperature (T_b)	3090 K
Density (ρ)	7800 kg/m^3
Thermal conductivity (k)	14 W/mK
Thermal diffusivity (α)	0.0000039 m^2/s
Heat capacity (C)	450 W/mK

It is appreciated, that when T is around 2500 K, all of the BRs give similar values for the tensile strength; this suggests that at this temperature, it is possible to increase BR with similar tensile strength as BR1 and BR2. At this value of T, which represents 55% of the range from Tm to Tb, it is possible to explore using a high BR (e.g. BR3) without compromising the tensile strength performance. Higher temperatures could be employed, but high cooling rates would then be present, which would induce cracking behaviour and hence a reduction in mechanical performance, as noted by Xiang et al. and Gao et al. [100, 146].

Table 4.5 shows that low scan speed values do not increase BR (e.g. BR_1), but it shows

shorter variations of mechanical properties than higher ones (e.g. BR_2 and BR_3), with the exception of wear rate.

Table 4.5: Mechanical performance variability according to BR

	Range of variability (max-min)		
Mechanical properties	BR1	BR2	BR3
Tensile strength MPa	485.22	347.18	271.46
Microhardness HV 0.5	49.4	25.89	20.3
Relative density	11.01	6.22	8.75
Flexural strength MPa	748.3	597.69	569.96
Torsional strength N m	14.93	13.12	10.51
Wear rate g Nm	0.48	1.78	1.02

4.1.5 Conclusions from processability study

The proposed processability strategy estimates the temperature of the melt pool during the process based on the characteristics of the metallic alloy powder for particular process parameters (i.e. a particular machine).

With this strategy the processability estimation was based on the BR for the LPBF-M process. This metric depends on the the characteristics of the material and process parameters employed. The results presented here suggest that it is necessary to identify the impact of modifying BR on the mechanical properties. All alloys have different temperature gradients, cooling rates, thermal stress, and melt pool dimensions due to the variation in the process parameters.

Processability analysis and its effects on mechanical performance were analysed and discussed. On the one hand, Oczsoy et al. [138] showed that it was possible to obtain full 17-4 PH dense components through LPBF-M with different P, v and h_d. Oczsoy et al. [138] presented partial mechanical test results, which did not allow to identify why the properties varied, even though the densities were higher than 99%.

On the other hand, Zhu et al. [142] studied the electrical consumption of the LPBF-M process and studied mechanical properties like tensile strength, relative density, flexural strength, hardness, torsional strength and wear rate. In this work, three different build rates were used: low, medium, and high, as a result of using three different scan velocities (v): 750, 857, and 1000 mm/s, with different P from 120 to 200 W and keeping l_t and h_d constant (50 um and 110 um, respectively). BR was presented as a graph chart according to the T achieved during the melting process. While is true that this author evaluated a spectrum of processability, h_d and l_t were extremely high, decreasing the bonding of the melting pool, therefore decreasing density.

Understanding the material process interaction of LPBF-M and its implications on the final mechanical properties is crucial for optimizing the manufacturing process and ensuring high-quality components. The combined insights from the above studies and further research in this area will pave the way for more informed decision-making and advancements in the field of additive manufacturing, particularly in the context of LPBF-M.

4.2 Manufacturability study

AM has enabled the possibility of constructing complex shapes with the potential to reduce material waste, cost, and the cycle of product development, opening new possibilities for engineering applications through geometrical flexibility, size and type of shapes, e.g., struts, and wall thickness. Nevertheless, complex shapes contain elements such as thin, inclined walls, and angled struts that stretch the capabilities of the process [69, 147].

The complexity of such structures, combined with the variability that exists in LPBF-M due to a wide range of material conditions and process parameters for each LPBF-M machine brand, creates uncertainty in whether a structure is manufacturable or not, since a part that is manufacturable in one machine may not necessarily be in another.

In this chapter, manufacturability is studied using an approach in which the minimum unit of the process, e.g. the melting pool, is geometrically compatible with the desired geometry. According to this approach, previous calculations of melt pool dimension enable the possibility of knowing the manufacturability of a complex structure according to the process parameters used.

4.2.1 Previous studies of Manufacturability of complex structures in the LPBF-M in literature

In order to solve technical problems (such as whether a structure is not manufacturable), it is necessary to consider the material, process and geometry. In practice, it is also necessary not only to solve the demands of the users, but the restrictions that the process entails to manufacture the component. Components ultimately built must meet the requirements to be considered successful in their respective markets [10, 148].

Complex structures such as heat exchangers, porous structures and optimized structures, enable unique physical, mechanical, acoustic and thermal properties, making them suitable for engineering applications in the medical, aerospace, automotive and energy fields. It is

worth to mentioning that manufacturing complex shapes through conventional manufacturing methods is hard. [60, 149–152].

The LPBF-M process allows the construction of metal lightweight structures due to its ability to build features in the micrometre order directly from the digital CAD model [68,153].

In order to achieve the full potential of LPBF-M, it is important to ensure that complex shapes are manufacturable. In theory, it is possible to build any geometry, however certain geometries are not manufacturable because these type of structures stretch the capabilities of the process with elements (overhangs, thin walls and struts) that eventually could cause failures and stoppages during manufacture, increasing costs and time [153–157].

Thus, there is an interest in knowing the geometrical limits like minimal thickness and angle of walls and struts for LPBF-M, since this process has limitations due to its powder-melted laser nature, powder adhesion, heat stress accumulation and structure collapse depending on the given geometry. It is difficult to predict if the manufacturability of a complex element will be successful with acceptable quality, among the main challenges using LPBF-M, are characteristics such as overhangs, thin walls and struts. [158, 159].

4.2.1.1 Overhangs

Overhang structures are areas of a part that are not supported by underlying layers and that are defined by an overhang angle and height [160]. These structures are inevitable in mechanical design; whenever they are built with LPBF-M, defects such as stair step effect, warping and dross appear near the surfaces, such defects are show in Figure 4.8 [157, 161]. Construction of overhangs without supports may result in deformed objects because the loose powder is not as thermally conductive as when manufactured with supports, since support structures constitute a thermal exchange path; this causes, the heat of the melt pool to be dissipated, and distortions and residual stresses are thus diminished. Support structures serve to fix the part to a built platform and avoid the collapse and deformation of the part. Support structures' disadvantages are increased building time and post-processing

operations that may damage the part [162–164]. It is recommended the use of support structures whenever surfaces are oriented 30-45° degrees above the build platform. However, this depends on the material used in the L-PBF along with the combination of manufacturing parameters [161, 165–167].

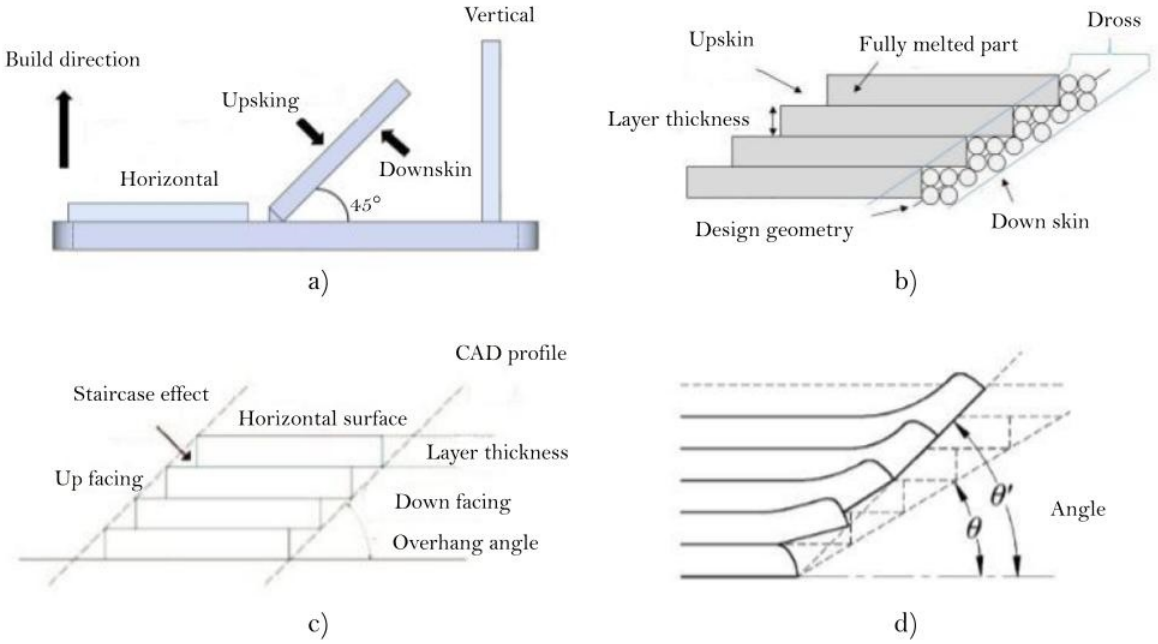

Figure 4.7: Defects in overhanging geometries. a) Example of overhang structure b) Dross formation and accumulation c) Stair step effect d) Warping [168–170].

4.2.1.2 Thin walls

Unlike solid parts (bulk parts) built using LPBF-M, building thin walls entails completely different construction conditions [171, 172]:

- Only vertical thermal cycles are repeated in an area in the order of μm^2 since the thin walls are formed from few melt pools.

- A heat transfer phenomenon appears because on both sides of the thin wall there is powder.
- An external stress is generated in a small area provoked by the scrapper when it deposits the powder multiple times.

Thin walls push the capabilities of L-PBF to the limit as they contain adhering unmelted powder, internal pores, cracks and shape irregularities [50, 171]. The study of thin walls has been carried out with different LPBF-M equipments and with distinct alloys. Yadroitsev et al. [173] identified that scanning strategy along the length of a thin wall (lengthwise direction) less than 1 mm is adequate to obtain thinner builds, achieving vertical walls in the range of 140-540 μ thickness with stainless steel 904L. Yang et al. [171] fabricated 200 μm thin vertical walls with Inconel 718, identifying that keyhole mode microstructure increased and so did hardness in the center of the thin wall.

Kranz et al. carried out an experimental investigation analysing the position of the components on the construction platform together with the orientation angle with respect to the powder dispensing (α) with an orientation of 0°,45°,90°,135° and 180°, with angles of inclination with respect to the construction platform (β) and its influence on the components quality [174]. This author suggested design guidelines of complex geometries, not only for thin walls, but also for cylinders, small holes and cantilever structures. In the case of thin walls, these were built with thickness of 0.2, 0.3, 0.4, 0.5, 0.6 and 0.7 mm. The 0.4 mm thick constructions showed a stable process and were completely built. The minimum angle with the minimum wall thickness was achieved at 30° and 0.3 mm, respectively.

Karim et al. [175] studied the limits of different complex geometries and proposed design guidelines for Inconel 718 alloy with fixed manufacturing parameters (P=200 W, v=1000 m/s, h_d=95μm,l_t=60μm) with a GE Additive M2 system (General Electric Additive, Lichtenfels, Germany). The geometries studied were short thin walls with and without support material, with constant with and height with different thickness. Results showed that it is not possible to build short thin walls smaller than 0.3 mm, while the limit for long thin walls

is 0.6 mm. All inclined thin walls are manufacturable to 25° of inclination, however, smaller angles were not explored.

4.2.1.3 Struts

The LPBF-M process has the potential to build metallic complex components such as reticulated structures. These kind of components can be built by conventional processes like investment casting and cutting, but it may need many steps to build them [176]. Reticulated structures are constituted by struts interconnected by nodes that form a unit cell which is repeated three-dimensionally. A reticulated structure designed with a tetrahedron unit cell, with dimensions of 200 x 200 x 200 mm^3, strut diameter of 0.5 mm and strut length of 5.0 mm, contains 260 000 inclined struts [177]. Therefore, its study is of great value, mainly because struts contain a variety of defects and imperfections. The area melted is different than that of "bulk solid components", which leads to different heat accumulation effects, these differences affect the manufacturability and mechanical performance of the entire component [178]. There is a disparity between the desined structure and the structure built built by LPBF-M Abele et al. Van Bael [179, 180] identify this may be due to: the melt pool is larger than the diameter of the laser spot, rugosity, shrinkage and powder adhered to the strut. This is shown on Figure

The study of manufacturability has been carried out experimentally to determine the minimum achievable strut diameter and inclination without the need for support structures [1]. Van Bael et al. [180] studied struts built with Ti6Al4V, with an in-house machine equipped with Yb:YAG fibre laser, with a diameter of 80 μ, using P of 42 W, v of 260 mm/s and l_t of 30 μm. This author achieved 0.2 mm diameter struts inclined at 45° and 90°. For the same alloy and inclinations, Hao et al. [181] stated that struts with diameters of 0.05 mm are possible using a Realizer SLM Workstation, with P of 95 W, v of 500 mm/s, h_d of 75 μm and l_of 75 μm. Mazur et al. [182] studied Ti6Al4V too, varying inclination from

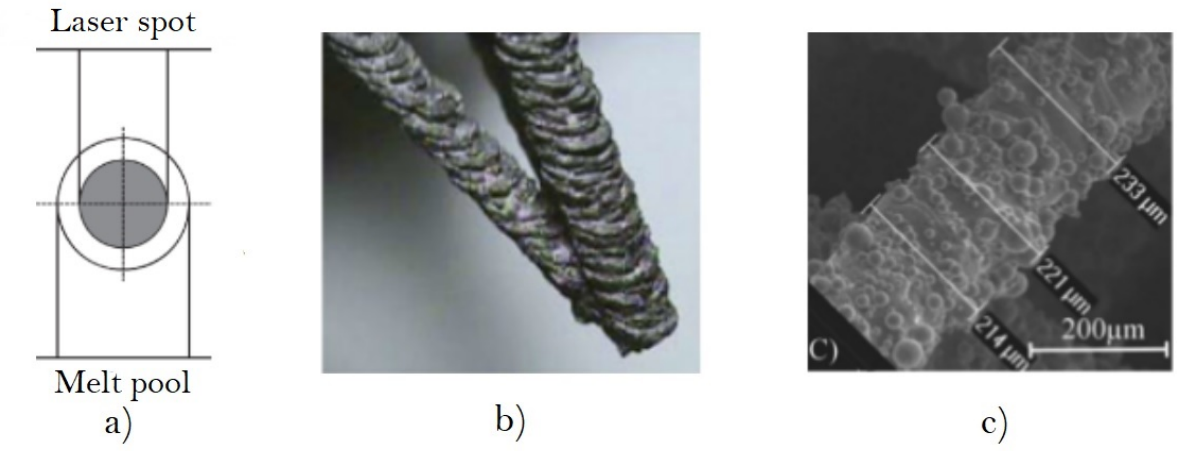

Figure 4.8: Reasons why there is a disparity between the designed structure and the tructure built by LPBF-M. a) Melting pool larger than the diameter of the laser spot b) Rugosity c) Powder adhered to structures [179, 180].

0 to 60°, with increments of 10°, and strut diameters from 0.3 to 1.0 mm, with increments of 0.1 mm, using an SLM250HL machine, with particle size of the powder of 40 μm, P of 175 W and v of 710 mm/s. With these process parameters and material characteristics, the minimum manufacturable strut angle was found to be achieved at 20° and 0.3 mm diameter. Leary et al. [1] studied struts made of AlSi10Mg at 0°, 35.3°, 45 and 90 with 0.5, 1.0, 2.0 and 3.0 mm in a SLM Solutions GMBH LPBF equipment,with P=350 W, h_d=0.19 mm, v=921.05 mm/s, l_t=50μm. Struts were manufacturable at any angle, except for horizontal struts (0° inclination) at any diameter, since the strut could not to be attached to the build plate and the recoater wiped it away.

4.2.2 Manufacturability approach through the fundamental unit

Manufacturability is defined as *the design characteristics which indicate how difficult or easy the design is from a manufacturing perspective* [4–6]. This has been studied for different conventional methods such as printing circuits, assembly and machining, with the objective of increasing competitiveness, reducing production time, identifying and solving manufacturing

problems. This is known as Design for Manufacturing (DfM) methodologies, with which the designers take into account manufacturing constraints so that, in product development, manufacturing problems are identified and alleviated with the objective of improving product quality [7–9].

In the case of AM this is different, due its layer by layer nature, AM reduces some DfM constraints of conventional manufacturing processes without the need of fixtures, tools, molds or any additional auxiliary step. In AM, designers must not take into account the process but exploit the advantages of the process in order to expand design freedom [50].

As a consequence, the concept manufacturability must be adapted for the additive LPBF process. For this, design for Additive manufacturing DfAM surged, and was defined as *The Synthesis of shapes, sizes, geometric mesostructures, and material compositions and microstructures to best utilize manufacturing process capabilities to achieve desired performance and other life-cycle objectives* [183].

Literature shows that exists studies of LPBF-M manufacturability of complex structures such as inclined struts and thin walls, holes and overhanging structures [171, 173]. Other authors offer design guidelines to help in their construction with different alloys [174, 175]. Nevertheless they are achievable under specific processes and parameters, therefore results might not be transferable if material characteristics change. For LPBF-M a range of material conditions and process parameters and being used for each specific machine, this has caused variation, not only in mechanical performance and part quality, but in manufacturability, given that a part that is manufacturable in one machine, may not necessarily be in another.

This research identified that the manufacturability of a complex structure has not yet been studied considering that the melting pool produced by the material-process interaction, is compatible with the desired geometry. For this reason, the definition of manufacturability for LPBF-M is proposed as:

Manufacturability*: Minimal achievable feature as a result of the combination of mate-*

rial conditions and process parameters, which is compatible with the geometry desired to be built, which allows for its complete construction, and meets the application quality requirements.

A manufacturability diagram is shown in Figure 4.9. On this Figure, processability is presented as the interaction of material with process that generates the melting pool, e.g the minimal unit, in addition, manufactruability is represented, where it is considered the melting pool as consequence of material-process interaction with the geometry for a thin strut.

4.2.3 Conclusions of Manufacturability study

LPBF-M has unlocked new frontiers in engineering by offering the potential to fabricate metallic intricate shapes, leading to reduced material waste, cost, and faster product development cycles. The versatility of AM allows for geometrical flexibility, accommodating a wide range of shapes, sizes, and features, such as struts and variable wall thicknesses. However, the inherent complexity of such structures, can push the limits of the manufacturing process.

The inherent complexity of such structures, combined with the inherent variability in Laser Powder Bed Fusion for Metals (LPBF-M) arising from the diverse material conditions and process parameters across different LPBF-M machine brands, creates uncertainty about the manufacturability of certain structures. What may be manufacturable on one machine could prove unfeasible on another, resulting in potential failures and interruptions during manufacturing, leading to increased costs and time constraints.

In order to unlock the full potential of LPBF-M, it becomes imperative to ensure that complex shapes are not only theoretically feasible but also practically manufacturable. While it is theoretically possible to build any desired geometry, not all geometries can be successfully manufactured within the capabilities of the LPBF-M process. Elements such as overhangs,

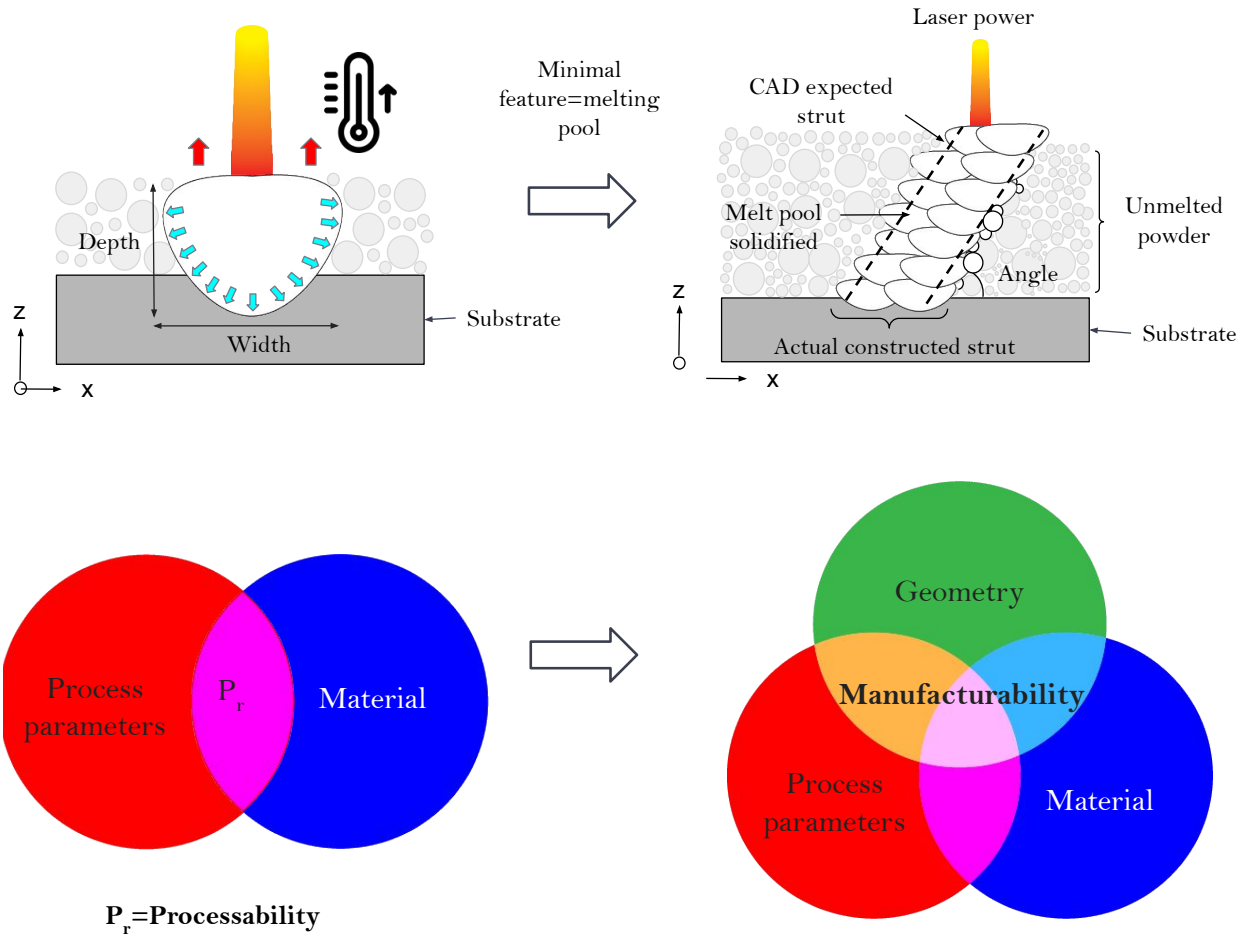

Figure 4.9: Manufacturability diagram with melt pool characteristics as a consequence of interaction between material conditions and process parameters

thin walls, and struts pose significant challenges due to the nature of the powder-melted laser process, powder adhesion, heat stress accumulation, and the risk of structure collapse depending on the given geometry. Understanding the geometrical limits, such as minimal thickness and angles of walls and struts, becomes essential to address these challenges and achieve high-quality manufacturing outcomes.

The approach presented in this section, proposes studying the manufacturability of complex structures through the fundamental unit of the process (the melting pool)and its geometric compatibility with the desired structure. By meticulously calculating the dimensions

of the melt pool, it is gained the valuable insights into the potential manufacturability of a complex element based on the specific process parameters employed. This help in guiding designers and engineers towards optimal process parameter selections to ensure successful and reliable manufacturing outcomes. Nonetheless, further experimentation and research are necessary to comprehensively address the challenges posed by overhangs, thin walls, struts, and reticulated structures with different cell units, ultimately advancing the state-of-the-art in LPBF-M and propelling its adoption across various industries.

4.3 Future work proposal for Processability and Manufacturability

From the study of processability, the effects on mechanical performace when equal temperatures are achieved through different combinations of P and v within the processability region and the effects on construction at equal build rates and differente temperatures were both unclear.

Therefore, components are proposed to be built according to the chart shown in Figure 4.10, this Figure shows the conditions inside the potential processability under which the components will be studied taking into account five different temperatures T (T_1, T_2, T_3, T_4 and T_5) and five different BR (BR_1, BR_2, BR_3, BR_4 and BR_5), this chart is made modifying P and v, fixing h_d and l_t.

17-4 stainless steel alloy will be used to manufacture vertical ASTM E8 standar specimens to characterize tensile behaviour, density and roughness. A 3D Systems ProX DMP 320 machine will carry out the construction of components under and argon protect atmosphere. Static tensile tests will be performed in a Shimadzu AGS-X 50 KN universal tensile frame machine.

One of the objectives of this experimentation is to determine the effect of temperature on the mechanical properties of the components. Since it is not identified in literature at which

temperature intervals it is advisable to operate in the LPBF-M, as typically, P and v are changed without taking into account the temperature and dimension pools.

Another objective is to determine the effects of increasing the BR on the mechanical properties, density and microstructure. Since "high" P or v would generate faster cooling rate, thermal stress and cracking, Xiao et al. [184] identified that v has a more significant effect than P and h_d in residual stress; this would affect not only the integrity of the built part, but also its appearance, as the induced thermal effect provokes warping on the built part, which might need a post-process operation in order to alleviate the defect, this may not be practical for parts that are willing to be used as they are built.

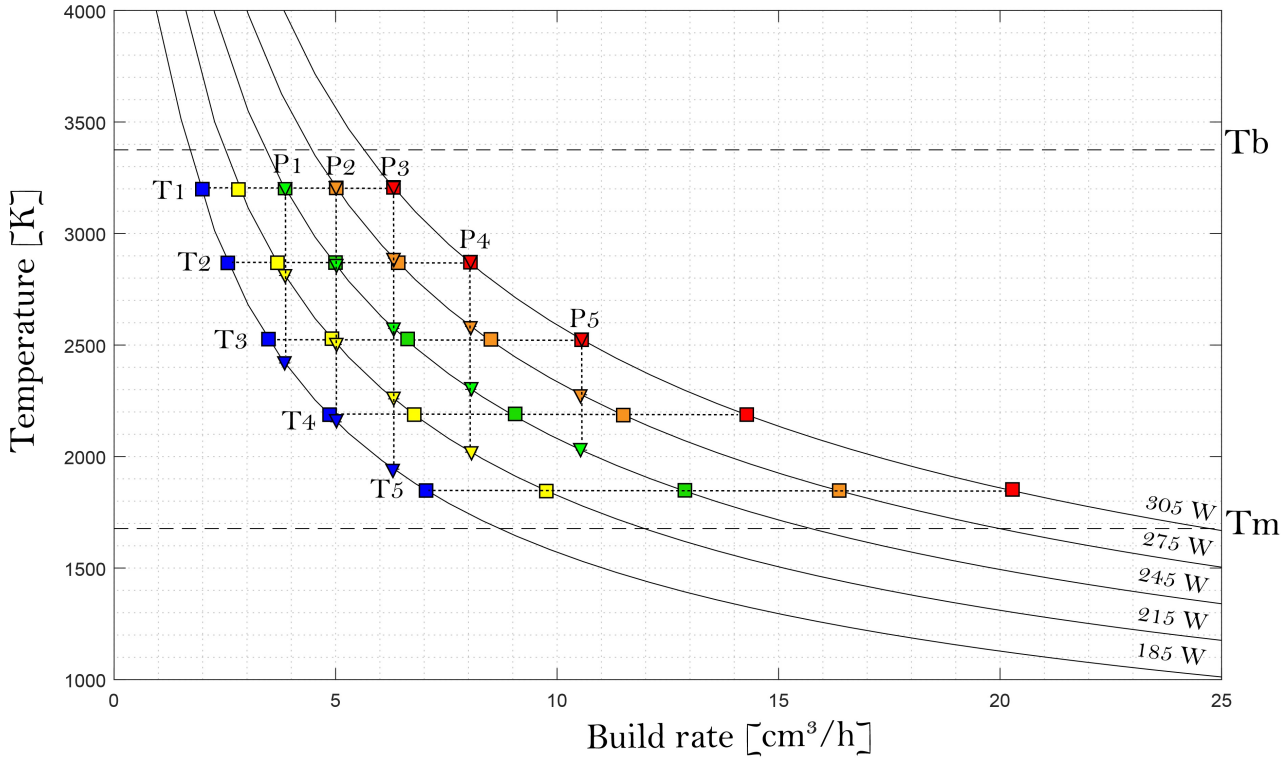

Figure 4.10: Process parameters for the processability experimental study.

In the case of Manufacturability, it is proposed the study of thin structures and different process parameters based the proposal experimentation of processability (Figure 4.10).

When modifying P and v, melting pool dimensions are modified too, based on this, it is possible to configure the number of melting pools in thin structures as shown on Figure 4.11, which shows a thin geometry made up of a single melting pool that encompasses the expected design geometry (Figure 4.11a), it is also shown the same thin geometry made up with two smaller melting pools, as well as made of closer multiple ones (Figure 4.11b and 4.11c), in this case the h_d is modified to fit in the expected design thin geometry. Figures 4.11d-f indicate deeper melting pools using , keeping l_t and h_d fixed.

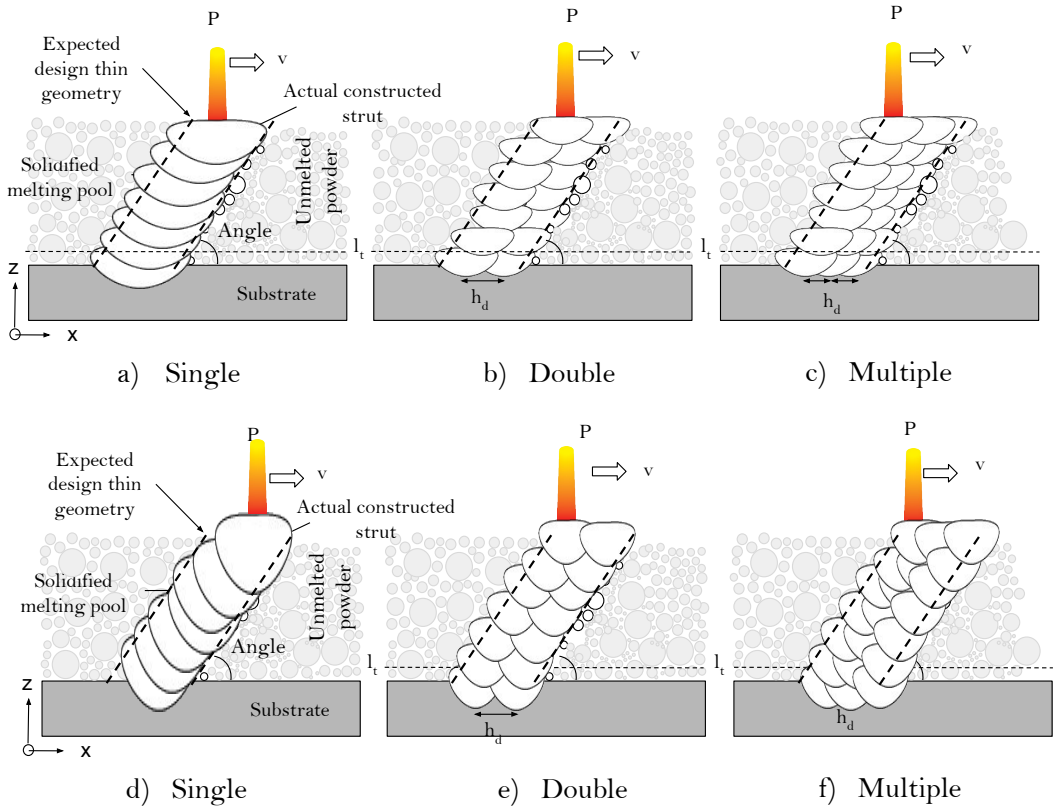

Figure 4.11: Manufacturability proposal for the study of thin angled structure made up of a) Single b) Double and c) Multiple "small" melting pools d) Single e) Double and f) Multiple "deeper" melting pools.

The proposed processability strategy allows to estimate the characteristics of the fundamental unit of LPBF-M, in terms of melting pools dimensions, temperature and build rate, which help to identify the goemetrycal limits resulting from material-process interaction. It

is not reported on literature, the number of convenient melting pools to build a thin structure (e.g. it if is convenient to use one big or multiple close small ones) and, with that number of melt pools, which are their effects when the thin geometry angle is varied. Based on metrics of melting pool dimensions, temperature and build rate, it will be known the effects of increasing productivity (high v) when constructing this kind of geometries, as well as the effects of proccesing with high temperatures (high P).

With this approach, it is pretended to evaluate the manufacturability of thin angled struts and walls, as shown in Figure 4.12 modifying angle from 10° to 45°, and diameter and thickness from 0.1-1 mm.proposed, as well as its integrity defined in literature as *The condition which exists when a structure is sound and unimpaired in providing the desired level of structural safety, performance, durability, and supportability* [185].

Based on the results, a series of recommendations of process parameters according to material characteristics will be given to achieve melting pools compatible with the geometry desired, enabling the possibility of predicting the manufacturability of a complex structure.

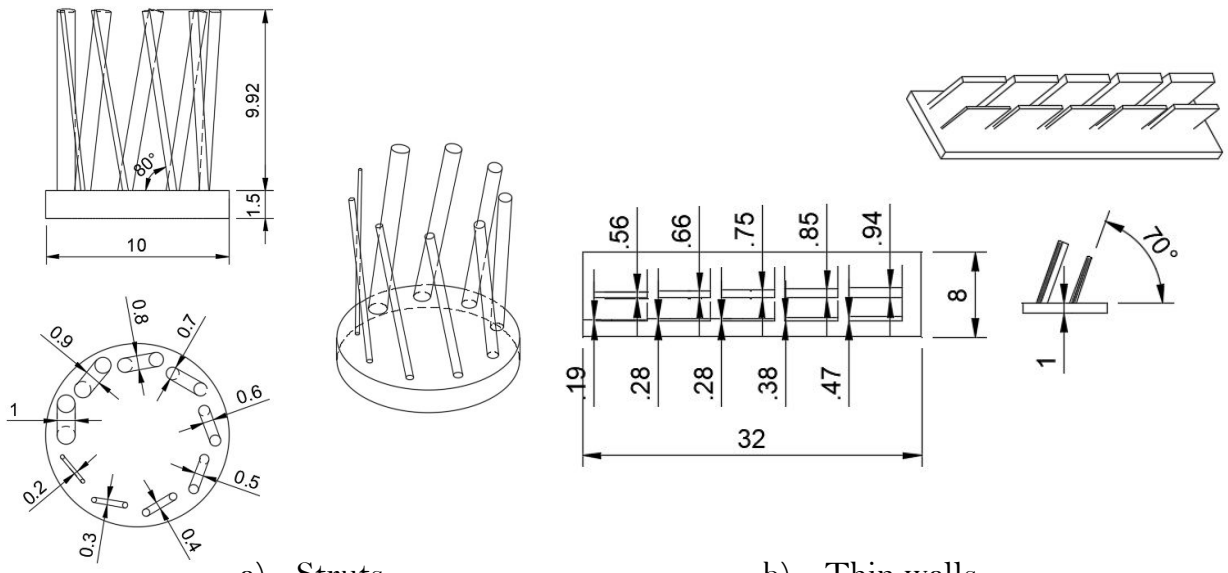

a) Struts b) Thin walls

Figure 4.12: Geometries proposed for the manufacturability study a) Struts b) Thin walls.

Chapter 5

Conclusions

Variability has held back the adoption of LPBF-M technology at the industrial level. One of the reasons is that, according to literature research, there is a range of parameters used by each machine brand according to their powder material characteristics. Based on this, processability was defined for LPBF-M as the material-process interaction; this concept was used to complement the study of manufacturability for LPBF-M, where the melt pool is compatible with the geometry desired.

The proposed strategy for quantifying the processability, consider the material characteristics and the process parameters, with which the processability concept for LPBF-M was proposed, together with a way to quantify it graphically was proposed too (Figure 4.2). Based on two research documents from the literature, exploration of the processability study was made and one experimental procedure was proposed.

From the first document, Ocsoy et al. [138] explored the possibility of manufacturing components varying P, v and h_d, obtaining stainless steel 17-4 PH components with a 99% relative density.. However, the presented results did not allow to identify why some components had higher tensile performance if all of them were fully dense.

In the second document, Zhu et al. [142], analyzed processability and its effects on tensile strength, relative density, flexural strength, hardness, torsional strength and wear rate per-

formance. Three build rates were calculated as a result of using different scan velocities with l_t and h_d constant. Build rate, temperature and mechanical properties were plotted. From literature analysis, this has not been previously compared. These charts elucidate that, with the material characteristics and process parameters employed, it is possible to speed the construction by up to 30% (with BR_1 achieving similar mechanical performance (hardness, torsional strength and wear rate) than with BR_3 and BR_2, overcoming them (as is the case for tensile strength).

An opportunity to study processability with lower values than Zhu et al. is identified, like h_d and l_t, allowing the study of denser samples at equal temperatures with different combinations of P and v and its implications on mechanical performance. Users may take into account processability depending on the application in order to speed up productivity.

Through the study of processability proposed, it is possible explain why there is the variability that exists in LPBF-M as different material characteristics and process parameters are used. With analytical equations, it is possible to estimate melt pool dimensions and temperature in order to predict processability and visualize it with the help of the diagram proposed in this work.

In the case of the manufacturability study, it is proposed its study through the proposed processability strategy, which allows to estimate the fundamental unit of LPBF-M, based on its dimensions, temperature and build rate. According to this proposal, it will help to determine the geometrical limits resulting from the material-process interaction, enabling the possibility of predicting the manufacturability of complex structure.

Bibliography

[1] M. Leary, M. Mazur, J. Elambasseril, M. McMillan, T. Chirent, Y. Sun, M. Qian, M. Easton, and M. Brandt, "Selective laser melting (slm) of alsi12mg lattice structures," *Materials & Design*, vol. 98, pp. 344–357, 2016.

[2] A. Grossmann, J. Felger, T. Froelich, J. Gosmann, and C. Mittelstedt, "Melt pool controlled laser powder bed fusion for customised low-density lattice structures," *Materials & Design*, vol. 181, p. 108054, 2019.

[3] S. Kalpakjian and S. R. Schmid, "Manufacturing engineering and technology (p. 913)," *Upper Saddle River, NJ, USA: Pearson*, 2014.

[4] D. R. Eyers and A. T. Potter, "Industrial additive manufacturing: A manufacturing systems perspective," *Computers in industry*, vol. 92, pp. 208–218, 2017.

[5] J. Parnaby, "Concept of a manufacturing system," *International Journal of Production Research*, vol. 17, no. 2, pp. 123–135, 1979.

[6] J. Parnaby and D. R. Towill, "Exploiting the concept of a manufacturing system part i: The relationship with process control," *Journal of Manufacturing Technology Management*, vol. 20, no. 7, pp. 915–932, 2009.

[7] S. K. Gupta, *Automated manufacturability analysis of machined parts*. PhD thesis, 1995.

[8] S. K. Gupta and D. S. Nau, "Systematic approach to analysing the manufacturability of machined parts," *Computer-Aided Design*, vol. 27, no. 5, pp. 323–342, 1995.

[9] N. Yannoulakis, S. Joshi, and R. Wysk, "Quantitative measures of manufacturability for rotational parts," 1994.

[10] Y. Zhang, S. Yang, and Y. F. Zhao, "Manufacturability analysis of metal laser-based powder bed fusion additive manufacturing—a survey," *The International Journal of Advanced Manufacturing Technology*, vol. 110, pp. 57–78, 2020.

[11] D. M. Anderson, *Design for manufacturability & concurrent engineering: how to design for low cost, design in high quality, design for lean manufacture, and design quickly for fast production*. CIM press, 2003.

[12] D. M. Anderson, *Design for manufacturability: how to use concurrent engineering to rapidly develop low-cost, high-quality products for lean production*. CRC press, 2020.

[13] B. P. Conner, G. P. Manogharan, A. N. Martof, L. M. Rodomsky, C. M. Rodomsky, D. C. Jordan, and J. W. Limperos, "Making sense of 3-d printing: Creating a map of additive manufacturing products and services," *Additive manufacturing*, vol. 1, pp. 64–76, 2014.

[14] H. Bikas, P. Stavropoulos, and G. Chryssolouris, "Additive manufacturing methods and modelling approaches: a critical review," *The International Journal of Advanced Manufacturing Technology*, vol. 83, pp. 389–405, 2016.

[15] I. G. Ian Gibson, "Additive manufacturing technologies 3d printing, rapid prototyping, and direct digital manufacturing," 2015.

[16] W. Gao, Y. Zhang, D. Ramanujan, K. Ramani, Y. Chen, C. B. Williams, C. C. Wang, Y. C. Shin, S. Zhang, and P. D. Zavattieri, "The status, challenges, and future of

additive manufacturing in engineering," *Computer-Aided Design*, vol. 69, pp. 65–89, 2015.

[17] L. S. Balanzar, "Modelo para predecir propiedades mecánicas en componentes fabricados por manufactura aditiva mediante el método de los elementos finitos," *Tesis UNAM*, vol. 1, p. 1, 2022.

[18] D. D. Gu, W. Meiners, K. Wissenbach, and R. Poprawe, "Laser additive manufacturing of metallic components: materials, processes and mechanisms," *International materials reviews*, vol. 57, no. 3, pp. 133–164, 2012.

[19] F. Laverne, F. Segonds, N. Anwer, and M. Le Coq, "Assembly based methods to support product innovation in design for additive manufacturing: an exploratory case study," *Journal of Mechanical Design*, vol. 137, no. 12, p. 121701, 2015.

[20] ISO/ASTM, "Iso/astm 52900: 2015 additive manufacturing-general principles-terminology," *ISO/ASTM*, vol. 1, no. 1, p. 1, 2015.

[21] P. Konda Gokuldoss, S. Kolla, and J. Eckert, "Additive manufacturing processes: Selective laser melting, electron beam melting and binder jetting—selection guidelines," *materials*, vol. 10, no. 6, p. 672, 2017.

[22] X. Xu, S. Meteyer, N. Perry, and Y. F. Zhao, "Energy consumption model of binder-jetting additive manufacturing processes," *International Journal of Production Research*, vol. 53, no. 23, pp. 7005–7015, 2015.

[23] K. V. Wong and A. Hernandez, "A review of additive manufacturing," *International scholarly research notices*, vol. 2012, 2012.

[24] M. Armstrong, H. Mehrabi, and N. Naveed, "An overview of modern metal additive manufacturing technology," *Journal of Manufacturing Processes*, vol. 84, pp. 1001–1029, 2022.

[25] S. Rouf, A. Malik, N. Singh, A. Raina, N. Naveed, M. I. H. Siddiqui, and M. I. U. Haq, "Additive manufacturing technologies: industrial and medical applications," *Sustainable Operations and Computers*, vol. 3, pp. 258–274, 2022.

[26] W. Bihlman, *A Methodology to Predict the Impact of Additive Manufacturing on the Aerospace Supply Chain.* PhD thesis, Purdue University Graduate School, 2020.

[27] B. Dovgyy, *Assessing the printability of alloys in fusion-based additive manufacturing: towards criteria for alloy selection.* PhD thesis, Imperial College London, 2022.

[28] L. J. Tan, W. Zhu, and K. Zhou, "Recent progress on polymer materials for additive manufacturing," *Advanced Functional Materials*, vol. 30, no. 43, p. 2003062, 2020.

[29] S. C. Ligon, R. Liska, J. Stampfl, M. Gurr, and R. Mulhaupt, "Polymers for 3d printing and customized additive manufacturing," *Chemical reviews*, vol. 117, no. 15, pp. 10212–10290, 2017.

[30] Y. L. Yap, C. Wang, S. L. Sing, V. Dikshit, W. Y. Yeong, and J. Wei, "Material jetting additive manufacturing: An experimental study using designed metrological benchmarks," *Precision engineering*, vol. 50, pp. 275–285, 2017.

[31] S. Tyagi, A. Yadav, and S. Deshmukh, "Review on mechanical characterization of 3d printed parts created using material jetting process," *Materials Today: Proceedings*, vol. 51, pp. 1012–1016, 2022.

[32] A. Elkaseer, K. J. Chen, J. C. Janhsen, O. Refle, V. Hagenmeyer, and S. G. Scholz, "Material jetting for advanced applications: A state-of-the-art review, gaps and future directions," *Additive Manufacturing*, p. 103270, 2022.

[33] C. Sandre, L. S. De Bernardez, L. Poggi, and J. M. Sanguinetti, "Application of material jetting technology for the development of incision and closure surgical devices," *Materials Today: Proceedings*, vol. 70, pp. 673–677, 2022.

[34] Y. L. Tee, P. Tran, M. Leary, P. Pille, and M. Brandt, "3d printing of polymer composites with material jetting: Mechanical and fractographic analysis," *Additive Manufacturing*, vol. 36, p. 101558, 2020.

[35] P. Lakkala, S. R. Munnangi, S. Bandari, and M. Repka, "Additive manufacturing technologies with emphasis on stereolithography 3d printing in pharmaceutical and medical applications: A review," *International Journal of Pharmaceutics: X*, p. 100159, 2023.

[36] R. Mahamood, S. Akinlabi, M. Shatalov, E. Murashkin, and E. Akinlabi, "Additive manufacturing/3d printing technology: A review," *Annals of "Dunarea de Jos" University of Galati. Fascicle XII, Welding Equipment and Technology*, vol. 30, pp. 51–58, 2019.

[37] P. M. Bhatt, A. M. Kabir, M. Peralta, H. A. Bruck, and S. K. Gupta, "A robotic cell for performing sheet lamination-based additive manufacturing," *Additive Manufacturing*, vol. 27, pp. 278–289, 2019.

[38] R. Friel, "Power ultrasonics for additive manufacturing and consolidating of materials," in *Power Ultrasonics*, pp. 313–335, Elsevier, 2015.

[39] A. Alammar, J. C. Kois, M. Revilla-León, and W. Att, "Additive manufacturing technologies: current status and future perspectives," *Journal of Prosthodontics*, vol. 31, no. S1, pp. 4–12, 2022.

[40] P. Ninpetch, P. Kowitwarangkul, S. Mahathanabodee, P. Chalermkarnnon, and P. Ratanadecho, "A review of computer simulations of metal 3d printing," in *AIP Conference Proceedings*, vol. 2279, p. 050002, AIP Publishing LLC, 2020.

[41] O. Diegel, A. Nordin, and D. Motte, *A practical guide to design for additive manufacturing*. Springer, 2019.

[42] M. Leary, *Design for additive manufacturing*. Elsevier, 2019.

[43] U. Ali, Y. Mahmoodkhani, S. I. Shahabad, R. Esmaeilizadeh, F. Liravi, E. Sheydaeian, K. Y. Huang, E. Marzbanrad, M. Vlasea, and E. Toyserkani, "On the measurement of relative powder-bed compaction density in powder-bed additive manufacturing processes," *Materials & Design*, vol. 155, pp. 495–501, 2018.

[44] S. Patel and M. Vlasea, "Melting modes in laser powder bed fusion," *Materialia*, vol. 9, p. 100591, 2020.

[45] X. Zhao, S. Li, M. Zhang, Y. Liu, T. B. Sercombe, S. Wang, Y. Hao, R. Yang, and L. E. Murr, "Comparison of the microstructures and mechanical properties of ti–6al–4v fabricated by selective laser melting and electron beam melting," *Materials & Design*, vol. 95, pp. 21–31, 2016.

[46] L. Dall'Ava, H. Hothi, A. Di Laura, J. Henckel, and A. Hart, "3d printed acetabular cups for total hip arthroplasty: a review article," *Metals*, vol. 9, no. 7, p. 729, 2019.

[47] N. Pushilina, M. Syrtanov, E. Kashkarov, T. Murashkina, V. Kudiiarov, R. Laptev, A. Lider, and A. Koptyug, "Influence of manufacturing parameters on microstructure and hydrogen sorption behavior of electron beam melted titanium ti-6al-4v alloy," *Materials*, vol. 11, no. 5, p. 763, 2018.

[48] M. Lopez, C. Pickett, E. Arrieta, L. E. Murr, R. B. Wicker, M. Ahlfors, D. Godfrey, and F. Medina, "Effects of postprocess hot isostatic pressing treatments on the mechanical performance of ebm fabricated ti-6al-2sn-4zr-2mo," *Materials*, vol. 13, no. 11, p. 2604, 2020.

[49] M. Mehrpouya, D. Tuma, T. Vaneker, M. Afrasiabi, M. Bambach, and I. Gibson, "Multimaterial powder bed fusion techniques," *Rapid prototyping journal*, 2022.

[50] F. Calignano, G. Cattano, and D. Manfredi, "Manufacturing of thin wall structures in alsi10mg alloy by laser powder bed fusion through process parameters," *Journal of Materials Processing Technology*, vol. 255, pp. 773–783, 2018.

[51] I. Yadroitsev, I. Yadroitsava, A. Du Plessis, and E. MacDonald, *Fundamentals of laser powder bed fusion of metals*. Elsevier, 2021.

[52] M. A. Obeidi, "Metal additive manufacturing by laser-powder bed fusion: Guidelines for process optimisation," *Results in Engineering*, vol. 15, p. 100473, 2022.

[53] T. Delacroix, F. Lomello, F. Schuster, H. Maskrot, and J.-P. Garandet, "Influence of powder recycling on 316l stainless steel feedstocks and printed parts in laser powder bed fusion," *Additive Manufacturing*, vol. 50, p. 102553, 2022.

[54] B. Kianian, *Wohlers Report 2019: 3D Printing and Additive Manufacturing State of the Industry, Annual Worldwide Progress Report: Chapter title: Middle East: Iran*. Wohlers Associates, Inc., 2019.

[55] T. Rockstroh, D. Abbott, K. Hix, and J. Mook, "Additive manufacturing at ge aviation," *Industrial Laser Solutions for Manufacturing [online] http://www. industrial-lasers. com/articles/print*, vol. 28, 2013.

[56] L. Focus, "Additive manufacturing at ge aviation," 2022.

[57] T. E. S. agency, "Advanced manufacturing can 3d print lightweight antennas," 2019.

[58] Bugatti, "New eight piston monobloc brake caliper," 2018.

[59] BEGO, "Implant solutions," 2017.

[60] S.-I. Park, D. W. Rosen, S.-k. Choi, and C. E. Duty, "Effective mechanical properties of lattice material fabricated by material extrusion additive manufacturing," *Additive Manufacturing*, vol. 1, pp. 12–23, 2014.

[61] L. J. Gibson, M. F. Ashby, and B. A. Harley, *Cellular materials in nature and medicine*. Cambridge University Press, 2010.

[62] T. A. Schaedler and W. B. Carter, "Architected cellular materials," *Annual Review of Materials Research*, vol. 46, pp. 187–210, 2016.

[63] I. Duarte, N. Peixinho, A. Andrade-Campos, and R. Valente, "Special issue on cellular materials," *Science and Technology of Materials*, vol. 30, no. 1, pp. 1–3, 2018.

[64] F. Tamburrino, S. Graziosi, and M. Bordegoni, "The design process of additively manufactured mesoscale lattice structures: a review," *Journal of Computing and Information Science in Engineering*, vol. 18, no. 4, 2018.

[65] G. Dong, Y. Tang, and Y. F. Zhao, "A survey of modeling of lattice structures fabricated by additive manufacturing," *Journal of Mechanical Design*, vol. 139, no. 10, p. 100906, 2017.

[66] M. McMillan, M. Jurg, M. Leary, and M. Brandt, "Programmatic lattice generation for additive manufacture," *Procedia Technology*, vol. 20, pp. 178–184, 2015.

[67] S. Ahmadi, G. Campoli, S. A. Yavari, B. Sajadi, R. Wauthlé, J. Schrooten, H. Weinans, and A. Zadpoor, "Mechanical behavior of regular open-cell porous biomaterials made of diamond lattice unit cells," *Journal of the mechanical behavior of biomedical materials*, vol. 34, pp. 106–115, 2014.

[68] C. Qiu, S. Yue, N. J. Adkins, M. Ward, H. Hassanin, P. D. Lee, P. J. Withers, and M. M. Attallah, "Influence of processing conditions on strut structure and compressive properties of cellular lattice structures fabricated by selective laser melting," *Materials Science and Engineering: A*, vol. 628, pp. 188–197, 2015.

[69] R. Guerra Silva, M. J. Torres, J. Zahr Viñuela, and A. G. Zamora, "Manufacturing and characterization of 3d miniature polymer lattice structures using fused filament fabrication," *Polymers*, vol. 13, no. 4, p. 635, 2021.

[70] M. Mayerhofer, W. Lepuschitz, T. Hoebert, M. Merdan, M. Schwentenwein, and T. I. Strasser, "Knowledge-driven manufacturability analysis for additive manufacturing," *IEEE Open Journal of the Industrial Electronics Society*, vol. 2, pp. 207–223, 2021.

[71] O. Pannitz and J. T. Sehrt, "Transferability of process parameters in laser powder bed fusion processes for an energy and cost efficient manufacturing," *Sustainability*, vol. 12, no. 4, p. 1565, 2020.

[72] P. Nandwana, A. Plotkowski, R. Kannan, S. Yoder, and R. Dehoff, "Predicting geometric influences in metal additive manufacturing," *Materials Today Communications*, vol. 25, p. 101174, 2020.

[73] S. L. Sing, F. E. Wiria, and W. Y. Yeong, "Selective laser melting of lattice structures: A statistical approach to manufacturability and mechanical behavior," *Robotics and Computer-Integrated Manufacturing*, vol. 49, pp. 170–180, 2018.

[74] D. R. Clymer, J. Cagan, and J. Beuth, "Power–velocity process design charts for powder bed additive manufacturing," *Journal of Mechanical Design*, vol. 139, no. 10, p. 100907, 2017.

[75] J.-P. Kruth, B. Vandenbroucke, J. Van Vaerenbergh, and P. Mercelis, "Benchmarking of different sls/slm processes as rapid manufacturing techniques," in *Proceedings of the International Conference Polymers & Moulds Innovations PMI 2005*, 2005.

[76] U. S. Bertoli, A. J. Wolfer, M. J. Matthews, J.-P. R. Delplanque, and J. M. Schoenung, "On the limitations of volumetric energy density as a design parameter for selective laser melting," *Materials & Design*, vol. 113, pp. 331–340, 2017.

[77] I. Yadroitsev, *Selective laser melting: Direct manufacturing of 3D-objects by selective laser melting of metal powders.* LAP Lambert Academic Publishing, 2009.

[78] C. Kamath, B. El-Dasher, G. F. Gallegos, W. E. King, and A. Sisto, "Density of additively-manufactured, 316l ss parts using laser powder-bed fusion at powers up to 400 w," *The International Journal of Advanced Manufacturing Technology*, vol. 74, pp. 65–78, 2014.

[79] D. Gu and Y. Shen, "Balling phenomena in direct laser sintering of stainless steel powder: Metallurgical mechanisms and control methods," *Materials & Design*, vol. 30, no. 8, pp. 2903–2910, 2009.

[80] K. G. Prashanth, S. Scudino, T. Maity, J. Das, and J. Eckert, "Is the energy density a reliable parameter for materials synthesis by selective laser melting?," *Materials Research Letters*, vol. 5, no. 6, pp. 386–390, 2017.

[81] J. P. Oliveira, A. LaLonde, and J. Ma, "Processing parameters in laser powder bed fusion metal additive manufacturing," *Materials & Design*, vol. 193, p. 108762, 2020.

[82] N. Lavery, J. Cherry, S. Mehmood, H. Davies, B. Girling, E. Sackett, S. Brown, and J. Sienz, "Effects of hot isostatic pressing on the elastic modulus and tensile properties of 316l parts made by powder bed laser fusion," *Materials Science and Engineering: A*, vol. 693, pp. 186–213, 2017.

[83] C. Ni, Y. Shi, and J. Liu, "Effects of inclination angle on surface roughness and corrosion properties of selective laser melted 316l stainless steel," *Materials Research Express*, vol. 6, no. 3, p. 036505, 2018.

[84] J. Suryawanshi, K. Prashanth, and U. Ramamurty, "Mechanical behavior of selective laser melted 316l stainless steel," *Materials Science and Engineering: A*, vol. 696, pp. 113–121, 2017.

[85] D. Gu, M. Xia, and D. Dai, "On the role of powder flow behavior in fluid thermodynamics and laser processability of ni-based composites by selective laser melting," *International Journal of Machine Tools and Manufacture*, vol. 137, pp. 67–78, 2019.

[86] C. Zhao, B. Shi, S. Chen, D. Du, T. Sun, B. J. Simonds, K. Fezzaa, and A. D. Rollett, "Laser melting modes in metal powder bed fusion additive manufacturing," *Reviews of Modern Physics*, vol. 94, no. 4, p. 045002, 2022.

[87] M. Markl and C. Körner, "Multiscale modeling of powder bed–based additive manufacturing," *Annual Review of Materials Research*, vol. 46, pp. 93–123, 2016.

[88] Q. Guo, C. Zhao, L. I. Escano, Z. Young, L. Xiong, K. Fezzaa, W. Everhart, B. Brown, T. Sun, and L. Chen, "Transient dynamics of powder spattering in laser powder bed fusion additive manufacturing process revealed by in-situ high-speed high-energy x-ray imaging," *Acta Materialia*, vol. 151, pp. 169–180, 2018.

[89] N. Kouraytem, X. Li, R. Cunningham, C. Zhao, N. Parab, T. Sun, A. D. Rollett, A. D. Spear, and W. Tan, "Effect of laser-matter interaction on molten pool flow and keyhole dynamics," *Physical Review Applied*, vol. 11, no. 6, p. 064054, 2019.

[90] L. Thijs, K. Kempen, J.-P. Kruth, and J. Van Humbeeck, "Fine-structured aluminium products with controllable texture by selective laser melting of pre-alloyed alsi10mg powder," *Acta Materialia*, vol. 61, no. 5, pp. 1809–1819, 2013.

[91] M. Gäumann, S. Henry, F. Cleton, J.-D. Wagnière, and W. Kurz, "Epitaxial laser metal forming: analysis of microstructure formation," *Materials Science and Engineering: A*, vol. 271, no. 1-2, pp. 232–241, 1999.

[92] M. H. Farshidianfar, A. Khajepour, and A. P. Gerlich, "Effect of real-time cooling rate on microstructure in laser additive manufacturing," *Journal of Materials Processing Technology*, vol. 231, pp. 468–478, 2016.

[93] J. C. Heigel, B. M. Lane, and L. E. Levine, "In situ measurements of melt-pool length and cooling rate during 3d builds of the metal am-bench artifacts," *Integrating Materials and Manufacturing Innovation*, vol. 9, pp. 31–53, 2020.

[94] C. Zhao, Q. Guo, X. Li, N. Parab, K. Fezzaa, W. Tan, L. Chen, and T. Sun, "Bulk-explosion-induced metal spattering during laser processing," *Physical Review X*, vol. 9, no. 2, p. 021052, 2019.

[95] R. Pordzik and P. Woizeschke, "An experimental approach for the direct measurement of temperatures in the vicinity of the keyhole front wall during deep-penetration laser welding," *Applied Sciences*, vol. 10, no. 11, p. 3951, 2020.

[96] L. Zheng, Q. Zhang, H. Cao, W. Wu, H. Ma, X. Ding, J. Yang, X. Duan, and S. Fan, "Melt pool boundary extraction and its width prediction from infrared images in selective laser melting," *Materials & Design*, vol. 183, p. 108110, 2019.

[97] F. Verhaeghe, T. Craeghs, J. Heulens, and L. Pandelaers, "A pragmatic model for selective laser melting with evaporation," *Acta Materialia*, vol. 57, no. 20, pp. 6006–6012, 2009.

[98] H. Chen and D. Gu, "Effect of metallurgical defect and phase transition on geometric accuracy and wear resistance of iron-based parts fabricated by selective laser melting," *Journal of Materials Research*, vol. 31, no. 10, pp. 1477–1490, 2016.

[99] T. DebRoy and S. David, "Physical processes in fusion welding," *Reviews of modern physics*, vol. 67, no. 1, p. 85, 1995.

[100] Z. Xiang, M. Yin, G. Dong, X. Mei, and G. Yin, "Modeling of the thermal physical process and study on the reliability of linear energy density for selective laser melting," *Results in Physics*, vol. 9, pp. 939–946, 2018.

[101] A. Suzuki, R. Nishida, N. Takata, M. Kobashi, and M. Kato, "Design of laser parameters for selectively laser melted maraging steel based on deposited energy density," *Additive manufacturing*, vol. 28, pp. 160–168, 2019.

[102] O. Rehme and C. Emmelmann, "Reproducibility for properties of selective laser melting products," in *Proceedings of the Third International WLT-Conference on Lasers in Manufacturing*, pp. 227–232, Proc. Third Int. WLT-Conference Lasers Manuf. Munich, 2005.

[103] S. A. Khairallah, A. T. Anderson, A. Rubenchik, and W. E. King, "Laser powder-bed fusion additive manufacturing: Physics of complex melt flow and formation mechanisms of pores, spatter, and denudation zones," *Acta Materialia*, vol. 108, pp. 36–45, 2016.

[104] B. Zhang, Y. Li, and Q. Bai, "Defect formation mechanisms in selective laser melting: a review," *Chinese Journal of Mechanical Engineering*, vol. 30, pp. 515–527, 2017.

[105] X. Zhang, X. Dang, and L. Yang, "Study on balling phenomena in selective laser melting," *Laser and Optoelectronics Progress*, vol. 6, pp. 131–136, 2014.

[106] W. Xu, S. Sun, J. Elambasseril, Q. Liu, M. Brandt, and M. Qian, "Ti-6al-4v additively manufactured by selective laser melting with superior mechanical properties," *Jom*, vol. 67, pp. 668–673, 2015.

[107] B. Vrancken, L. Thijs, J.-P. Kruth, and J. Van Humbeeck, "Heat treatment of ti6al4v produced by selective laser melting: Microstructure and mechanical properties," *Journal of Alloys and Compounds*, vol. 541, pp. 177–185, 2012.

[108] A. Hussein, L. Hao, C. Yan, and R. Everson, "Finite element simulation of the temperature and stress fields in single layers built without-support in selective laser melting," *Materials & Design (1980-2015)*, vol. 52, pp. 638–647, 2013.

[109] I. Yadroitsev, I. Yadroitsava, P. Bertrand, and I. Smurov, "Factor analysis of selective laser melting process parameters and geometrical characteristics of synthesized single tracks," *Rapid Prototyping Journal*, vol. 18, no. 3, pp. 201–208, 2012.

[110] T. Eagar, N. Tsai, *et al.*, "Temperature fields produced by traveling distributed heat sources," *Welding journal*, vol. 62, no. 12, pp. 346–355, 1983.

[111] J.-D. Kim, "Prediction of the penetration depth in laser beam welding," *KSME journal*, vol. 4, pp. 32–39, 1990.

[112] W. E. King, H. D. Barth, V. M. Castillo, G. F. Gallegos, J. W. Gibbs, D. E. Hahn, C. Kamath, and A. M. Rubenchik, "Observation of keyhole-mode laser melting in laser powder-bed fusion additive manufacturing," *Journal of Materials Processing Technology*, vol. 214, no. 12, pp. 2915–2925, 2014.

[113] R. Seidgazov and F. K. Mirzade, "Threshold conditions for thermocapillary transition to deep penetration mode in selective laser melting of metal powder bed," in *IOP Conference Series: Materials Science and Engineering*, vol. 759, p. 012023, IOP Publishing, 2020.

[114] C. Teng, D. Pal, H. Gong, K. Zeng, K. Briggs, N. Patil, and B. Stucker, "A review of defect modeling in laser material processing," *Additive Manufacturing*, vol. 14, pp. 137–147, 2017.

[115] D. Hann, J. Iammi, and J. Folkes, "A simple methodology for predicting laser-weld properties from material and laser parameters," *Journal of Physics D: Applied Physics*, vol. 44, no. 44, p. 445401, 2011.

[116] P. Promoppatum and S.-C. Yao, "Analytical evaluation of defect generation for selective laser melting of metals," *The International Journal of Advanced Manufacturing Technology*, vol. 103, pp. 1185–1198, 2019.

[117] T. Mukherjee, J. Zuback, A. De, and T. DebRoy, "Printability of alloys for additive manufacturing," *Scientific reports*, vol. 6, no. 1, p. 19717, 2016.

[118] H. Eskandari Sabzi and P. E. Rivera-Díaz-del Castillo, "Defect prevention in selective laser melting components: compositional and process effects," *Materials*, vol. 12, no. 22, p. 3791, 2019.

[119] M. Tang, P. C. Pistorius, and J. L. Beuth, "Prediction of lack-of-fusion porosity for powder bed fusion," *Additive Manufacturing*, vol. 14, pp. 39–48, 2017.

[120] R. Li, J. Liu, Y. Shi, L. Wang, and W. Jiang, "Balling behavior of stainless steel and nickel powder during selective laser melting process," *The International Journal of Advanced Manufacturing Technology*, vol. 59, pp. 1025–1035, 2012.

[121] X. Zhou, X. Liu, D. Zhang, Z. Shen, and W. Liu, "Balling phenomena in selective laser melted tungsten," *Journal of Materials Processing Technology*, vol. 222, pp. 33–42, 2015.

[122] D. Rosenthal, "Mathematical theory of heat distribution during welding and cutting," *Welding journal*, vol. 20, no. 5, pp. 220s–234s, 1941.

[123] M. Tang, P. C. Pistorius, S. Narra, and J. L. Beuth, "Rapid solidification: selective laser melting of alsi10mg," *Jom*, vol. 68, pp. 960–966, 2016.

[124] A. V. Gusarov, S. N. Grigoriev, M. A. Volosova, Y. A. Melnik, A. Laskin, D. V. Kotoban, and A. A. Okunkova, "On productivity of laser additive manufacturing," *Journal of Materials Processing Technology*, vol. 261, pp. 213–232, 2018.

[125] S. Cacace and Q. Semeraro, "Improvement of slm build rate of a357 alloy by optimizing fluence," *Journal of Manufacturing Processes*, vol. 66, pp. 115–124, 2021.

[126] Q. Tan, Y. Liu, Z. Fan, J. Zhang, Y. Yin, and M.-X. Zhang, "Effect of processing parameters on the densification of an additively manufactured 2024 al alloy," *Journal of Materials Science & Technology*, vol. 58, pp. 34–45, 2020.

[127] R. Engeli, T. Etter, S. Hövel, and K. Wegener, "Processability of different in738lc powder batches by selective laser melting," *Journal of Materials Processing Technology*, vol. 229, pp. 484–491, 2016.

[128] M. Balbaa, A. Ghasemi, E. Fereiduni, M. Elbestawi, S. Jadhav, and J.-P. Kruth, "Role of powder particle size on laser powder bed fusion processability of alsi10mg alloy," *Additive Manufacturing*, vol. 37, p. 101630, 2021.

[129] C. Cosma, J. Kessler, A. Gebhardt, I. Campbell, and N. Balc, "Improving the mechanical strength of dental applications and lattice structures slm processed," *Materials*, vol. 13, no. 4, p. 905, 2020.

[130] A. Dev, A. K. Srivastava, and S. Karmakar, "New generation hybrid nanobiocatalysts: The catalysis redefined," in *Handbook of nanomaterials for industrial applications*, pp. 217–231, Elsevier, 2018.

[131] E. Kalinchev, "Controlling the processability of polymeric materials," *International Polymer Science and Technology*, vol. 29, no. 5, pp. 55–62, 2002.

[132] J. Cai, Z. Liu, B. Cao, X. Guan, S. Liu, and J. Zhao, "Simultaneous improvement of the processability and mechanical properties of polyamide-6 by chain extension in extrusion," *Industrial & Engineering Chemistry Research*, vol. 59, no. 32, pp. 14334–14343, 2020.

[133] L. Greenwald, E. Breinan, and B. Kear, "Heat transfer properties and microstructures of laser surface melted alloys," in *AIP Conference Proceedings*, vol. 50, pp. 189–204, American Institute of Physics, 1979.

[134] M. J. Ansari, D.-S. Nguyen, and H. S. Park, "Investigation of slm process in terms of temperature distribution and melting pool size: Modeling and experimental approaches," *Materials*, vol. 12, no. 8, p. 1272, 2019.

[135] Y. Mahmoodkhani, U. Ali, S. Imani Shahabad, A. Rani Kasinathan, R. Esmaeilizadeh, A. Keshavarzkermani, E. Marzbanrad, and E. Toyserkani, "On the measurement of effective powder layer thickness in laser powder-bed fusion additive manufacturing of metals," *Progress in Additive Manufacturing*, vol. 4, pp. 109–116, 2019.

[136] A. B. Spierings, N. Herres, and G. Levy, "Influence of the particle size distribution on surface quality and mechanical properties in am steel parts," *Rapid Prototyping Journal*, vol. 17, no. 3, pp. 195–202, 2011.

[137] A. B. Spierings and G. Levy, "Comparison of density of stainless steel 316l parts produced with selective laser melting using different powder grades," in *2009 International Solid Freeform Fabrication Symposium*, University of Texas at Austin, 2009.

[138] A. Ozsoy, E. Yasa, M. Keles, and E. B. Tureyen, "Pulsed-mode selective laser melting of 17-4 ph stainless steel: Effect of laser parameters on density and mechanical properties," *Journal of Manufacturing Processes*, vol. 68, pp. 910–922, 2021.

[139] J. Cherry, H. Davies, S. Mehmood, N. Lavery, S. Brown, and J. Sienz, "Investigation into the effect of process parameters on microstructural and physical properties of 316l stainless steel parts by selective laser melting," *The International Journal of Advanced Manufacturing Technology*, vol. 76, pp. 869–879, 2015.

[140] L. Tonelli, A. Fortunato, and L. Ceschini, "Cocr alloy processed by selective laser melting (slm): Effect of laser energy density on microstructure, surface morphology, and hardness," *Journal of Manufacturing Processes*, vol. 52, pp. 106–119, 2020.

[141] M. Ghayoor, K. Lee, Y. He, C.-h. Chang, B. K. Paul, and S. Pasebani, "Selective laser melting of 304l stainless steel: Role of volumetric energy density on the microstructure, texture and mechanical properties," *Additive Manufacturing*, vol. 32, p. 101011, 2020.

[142] Y. Zhu, T. Peng, G. Jia, H. Zhang, S. Xu, and H. Yang, "Electrical energy consumption and mechanical properties of selective-laser-melting-produced 316l stainless steel

samples using various processing parameters," *Journal of cleaner production*, vol. 208, pp. 77–85, 2019.

[143] S. Shrestha, T. Starr, and K. Chou, "A study of keyhole porosity in selective laser melting: single-track scanning with micro-ct analysis," *Journal of Manufacturing Science and Engineering*, vol. 141, no. 7, 2019.

[144] T. Niendorf, S. Leuders, A. Riemer, H. A. Richard, T. Tröster, and D. Schwarze, "Highly anisotropic steel processed by selective laser melting," *Metallurgical and materials transactions B*, vol. 44, pp. 794–796, 2013.

[145] M. L. Montero-Sistiaga, M. Godino-Martinez, K. Boschmans, J.-P. Kruth, J. Van Humbeeck, and K. Vanmeensel, "Microstructure evolution of 316l produced by hp-slm (high power selective laser melting)," *Additive Manufacturing*, vol. 23, pp. 402–410, 2018.

[146] P. Gao, W. Huang, H. Yang, G. Jing, Q. Liu, G. Wang, Z. Wang, and X. Zeng, "Cracking behavior and control of β-solidifying ti-40al-9v-0.5 y alloy produced by selective laser melting," *Journal of Materials Science & Technology*, vol. 39, pp. 144–154, 2020.

[147] Z. Wu, S. P. Narra, and A. Rollett, "Exploring the fabrication limits of thin-wall structures in a laser powder bed fusion process," *The International Journal of Advanced Manufacturing Technology*, vol. 110, no. 1-2, pp. 191–207, 2020.

[148] C. Emmelmann, D. Herzog, and J. Kranz, "Design for laser additive manufacturing," in *Laser additive manufacturing*, pp. 259–279, Elsevier, 2017.

[149] Y. Zhang and Y. F. Zhao, "A web-based automated manufacturability analyzer and recommender for additive manufacturing (mar-am) via a hybrid machine learning model," *Expert Systems with Applications*, vol. 199, p. 117189, 2022.

[150] C. Zhang, A. Banerjee, A. Hoe, A. Tamraparni, J. R. Felts, P. J. Shamberger, and A. Elwany, "Design for laser powder bed additive manufacturing of alsi12 periodic mesoscale lattice structures," *The International Journal of Advanced Manufacturing Technology*, vol. 113, pp. 3599–3612, 2021.

[151] G. Savio, S. Rosso, R. Meneghello, G. Concheri, *et al.*, "Geometric modeling of cellular materials for additive manufacturing in biomedical field: a review," *Applied bionics and biomechanics*, vol. 2018, 2018.

[152] M. F. Ashby and R. M. Medalist, "The mechanical properties of cellular solids," 1983.

[153] L. Ding, S. Tan, W. Chen, Y. Jin, Y. Sun, and Y. Zhang, "Development of a manufacturability predictor for periodic cellular structures in a selective laser melting process via experiment and ann modelling," *Virtual and Physical Prototyping*, vol. 17, no. 4, pp. 948–965, 2022.

[154] D. Thomas, *The development of design rules for selective laser melting*. PhD thesis, University of Wales, 2010.

[155] J.-P. Rudolph and C. Emmelmann, "Analysis of design guidelines for automated order acceptance in additive manufacturing," *Procedia Cirp*, vol. 60, pp. 187–192, 2017.

[156] Y. Oh, H. Ko, T. Sprock, W. Z. Bernstein, and S. Kwon, "Part decomposition and evaluation based on standard design guidelines for additive manufacturability and assemblability," *Additive Manufacturing*, vol. 37, p. 101702, 2021.

[157] D. Wang, Y. Yang, Z. Yi, and X. Su, "Research on the fabricating quality optimization of the overhanging surface in slm process," *The International Journal of Advanced Manufacturing Technology*, vol. 65, pp. 1471–1484, 2013.

[158] H. D. Budinoff and S. McMains, "Will it print: a manufacturability toolbox for 3d printing," *International Journal on Interactive Design and Manufacturing (IJIDeM)*, vol. 15, no. 4, pp. 613–630, 2021.

[159] D. Wang, S. Wu, Y. Bai, H. Lin, Y. Yang, and C. Song, "Characteristics of typical geometrical features shaped by selective laser melting," *Journal of Laser Applications*, vol. 29, no. 2, p. 022007, 2017.

[160] M. Muthusamy, S. Safaee, and R. K. Chen, "Additive manufacturing of overhang structures using moisture-cured silicone with support material," *Journal of Manufacturing and Materials Processing*, vol. 2, no. 2, p. 24, 2018.

[161] K. Q. Le, C. H. Wong, K. Chua, C. Tang, and H. Du, "Discontinuity of overhanging melt track in selective laser melting process," *International Journal of Heat and Mass Transfer*, vol. 162, p. 120284, 2020.

[162] W. Ameen, A. Al-Ahmari, and M. K. Mohammed, "Self-supporting overhang structures produced by additive manufacturing through electron beam melting," *The International Journal of Advanced Manufacturing Technology*, vol. 104, pp. 2215–2232, 2019.

[163] L. Li, T. Pan, X. Zhang, Y. Chen, W. Cui, L. Yan, and F. Liou, "Deformations and stresses prediction of cantilever structures fabricated by selective laser melting process," *Rapid Prototyping Journal*, 2021.

[164] J.-P. Järvinen, V. Matilainen, X. Li, H. Piili, A. Salminen, I. Mäkelä, and O. Nyrhilä, "Characterization of effect of support structures in laser additive manufacturing of stainless steel," *Physics Procedia*, vol. 56, pp. 72–81, 2014.

[165] H. Chen, D. Gu, J. Xiong, and M. Xia, "Improving additive manufacturing processability of hard-to-process overhanging structure by selective laser melting," *Journal of Materials Processing Technology*, vol. 250, pp. 99–108, 2017.

[166] G. Piscopo, A. Salmi, and E. Atzeni, "On the quality of unsupported overhangs produced by laser powder bed fusion," *International Journal of Manufacturing Research*, vol. 14, no. 2, pp. 198–216, 2019.

[167] D. Brackett, I. Ashcroft, and R. Hague, "Topology optimization for additive manufacturing," in *2011 International Solid Freeform Fabrication Symposium*, University of Texas at Austin, 2011.

[168] R. Gumbleton, R. Batson, K. Nai, and A. Porch, "Effect of build orientation and laser power on microwave loss in metal additive manufactured components," *IEEE Access*, vol. 9, pp. 44514–44520, 2021.

[169] D. Wang, Y. Yang, R. Liu, D. Xiao, and J. Sun, "Study on the designing rules and processability of porous structure based on selective laser melting (slm)," *Journal of Materials Processing Technology*, vol. 213, no. 10, pp. 1734–1742, 2013.

[170] A. Charles, A. Elkaseer, T. Müller, L. Thijs, M. Torge, V. Hagenmeyer, and S. Scholz, "A study of the factors influencing generated surface roughness of downfacing surfaces in selective laser melting," in *Proceedings of the World Congress on Micro and Nano Manufacturing (WCMNM), Portorož, Slovenia*, vol. 3, p. 5, 2018.

[171] H. Yang, J. Yang, W. Huang, Z. Wang, and X. Zeng, "The printability, microstructure, crystallographic features and microhardness of selective laser melted inconel 718 thin wall," *Materials & Design*, vol. 156, pp. 407–418, 2018.

[172] K. Lin, L. Yuan, and D. Gu, "Influence of laser parameters and complex structural features on the bio-inspired complex thin-wall structures fabricated by selective laser melting," *Journal of Materials Processing Technology*, vol. 267, pp. 34–43, 2019.

[173] I. Yadroitsev, P. Bertrand, and I. Smurov, "Parametric analysis of the selective laser melting process," *Applied surface science*, vol. 253, no. 19, pp. 8064–8069, 2007.

[174] J. Kranz, D. Herzog, and C. Emmelmann, "Design guidelines for laser additive manufacturing of lightweight structures in tial6v4," *Journal of Laser Applications*, vol. 27, no. S1, p. S14001, 2015.

[175] D. Herzog, K. Asami, C. Scholl, C. Ohle, C. Emmelmann, A. Sharma, N. Markovic, and A. Harris, "Design guidelines for laser powder bed fusion in inconel 718," *Journal of laser applications*, vol. 34, no. 1, p. 012015, 2022.

[176] D. Li, X. Zhang, R. Qin, J. Xu, D. Yue, and B. Chen, "Influence of processing parameters on alsi10mg lattice structure during selective laser melting: Manufacturing defects, thermal behavior and compression properties," *Optics & Laser Technology*, vol. 161, p. 109182, 2023.

[177] X. Zhang, H. Tang, J. Wang, L. Jia, Y. Fan, M. Leary, and M. Qian, "Additive manufacturing of intricate lattice materials: Ensuring robust strut additive continuity to realize the design potential," *Additive Manufacturing*, vol. 58, p. 103022, 2022.

[178] B. Zhang, X. Han, C. Chen, W. Zhang, H. Liao, and B. Chen, "Effect of the strut size and tilt angle on the geometric characteristics of selective laser melting alsi10mg," *Rapid Prototyping Journal*, vol. 27, no. 5, pp. 879–889, 2021.

[179] E. Abele, H. A. Stoffregen, K. Klimkeit, H. Hoche, and M. Oechsner, "Optimisation of process parameters for lattice structures," *Rapid Prototyping Journal*, vol. 21, no. 1, pp. 117–127, 2015.

[180] S. Van Bael, G. Kerckhofs, M. Moesen, G. Pyka, J. Schrooten, and J.-P. Kruth, "Micro-ct-based improvement of geometrical and mechanical controllability of selective laser melted ti6al4v porous structures," *Materials Science and Engineering: A*, vol. 528, no. 24, pp. 7423–7431, 2011.

[181] L. Hao, D. Raymont, C. Yan, A. Hussein, and P. Young, "Design and additive manufacturing of cellular lattice structures," in *The International Conference on Advanced*

Research in Virtual and Rapid Prototyping (VRAP). Taylor & Francis Group, Leiria, pp. 249–254, 2011.

[182] M. Mazur, M. Leary, S. Sun, M. Vcelka, D. Shidid, and M. Brandt, "Deformation and failure behaviour of ti-6al-4v lattice structures manufactured by selective laser melting (slm)," *The International Journal of Advanced Manufacturing Technology*, vol. 84, pp. 1391–1411, 2016.

[183] D. W. Rosen, "Computer-aided design for additive manufacturing of cellular structures," *Computer-Aided Design and Applications*, vol. 4, no. 5, pp. 585–594, 2007.

[184] Z. Xiao, C. Chen, H. Zhu, Z. Hu, B. Nagarajan, L. Guo, and X. Zeng, "Study of residual stress in selective laser melting of ti6al4v," *Materials & Design*, vol. 193, p. 108846, 2020.

[185] M. Gorelik, "Additive manufacturing in the context of structural integrity," *International Journal of Fatigue*, vol. 94, pp. 168–177, 2017.